Master of Science Thesis

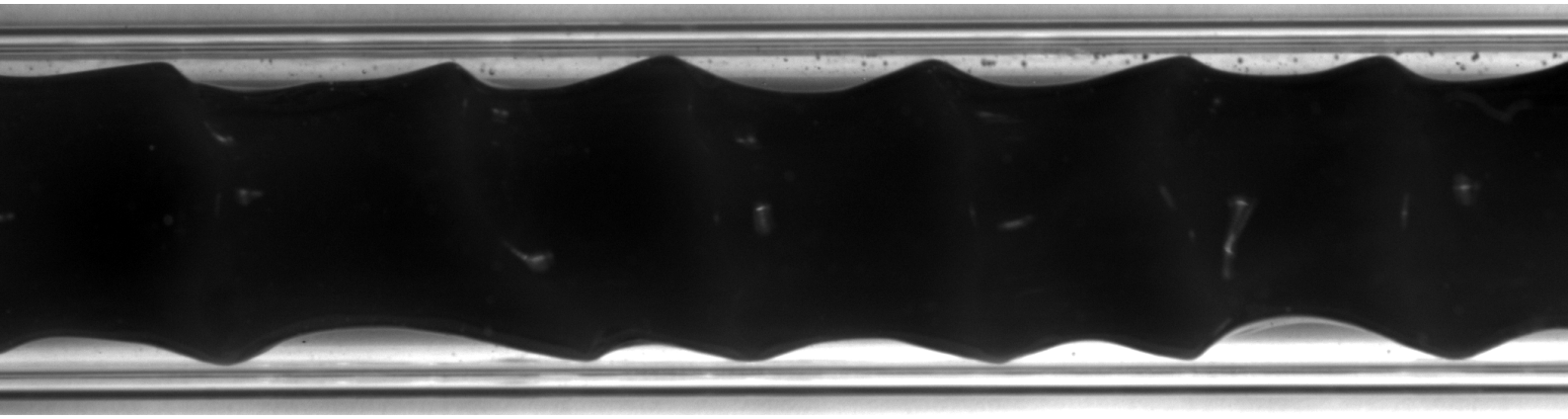

Influence of oil viscosity on oil-water core-annular flow through a horizontal pipe

H.J. van Duin

August 25, 2017

Aerodynamics

Faculty of Aerospace Engineering

TU Delft

Delft University of Technology

Influence of oil viscosity on oil-water core-annular flow through a horizontal pipe

Master of Science Thesis

For obtaining the degree of Master of Science in Aerospace Engineering
at Delft University of Technology

H.J. van Duin

August 25, 2017

Faculty of Aerospace Engineering · Delft University of Technology

Delft University of Technology

DELFT UNIVERSITY OF TECHNOLOGY
DEPARTMENT OF AERODYNAMICS

The undersigned hereby certify that they have read and recommend to the Faculty of Aerospace Engineering for acceptance the thesis entitled **"Influence of oil viscosity on oil-water core-annular flow through a horizontal pipe"** by **Hendrikus Johannis van Duin** in fulfilment of the requirements for the degree of **Master of Science**.

Dated: August 25, 2017

Examination committee:

Prof. dr. ir. R.A.W.M. Henkes

Prof. dr. ir. G. Ooms

Dr. ir. B.W. van Oudheusden

Dr. ir. A.H. van Zuijlen

Abstract

Transportation of very viscous fluids through pipelines is a real challenge. With the depletion of light oils in reservoirs, it becomes economically favourable to harvest heavy crude oils to contribute to meeting the ever growing energy demand. A suitable candidate for the transportation of these very viscous oil is by means of core-annular flow. Core-annular flow is a flow regime of liquid-liquid two-phase flow, where a low viscous fluid in the annulus (water) is used to lubricate a high viscous fluid in the core (oil). The pressure drop is considerably reduced compared to single phase oil flow at the same oil flow rate.

In this study the influence of the oil viscosity on oil-water core-annular flow through a horizontal pipe is investigated experimentally. The fixed oil flow rate is set at 0.35 l/s at which the watercut is varied between 9% and 25% and the oil kinematic viscosity is altered by heating up the oil in a range from 3000 cSt at 20 °C to 400 cSt at 50 °C. Pressure drop measurements for stable core-annular flow are recorded with an electronic pressure transducer and are scaled with the calculated pressure drop of single phase oil flow.

Results for the scaled pressure drop at room temperature are compared to results by Ingen Housz et al. It is concluded that for increasing oil-water viscosity ratio, the scaled pressure drop decreases. At the highest considered viscosity ratio, the scaled pressure drop is almost independent of the watercut. Two models to predict the pressure drop (by Brauner and by Bannwart) are evaluated and deviations between the models and measurements are discussed. Visualisation by means of high-speed camera is applied, where a mirror is placed on top of the visualisation section to capture the front and top view simultaneously. For decreasing oil viscosity, the oil-water interface shows a more irregular wave pattern with shorter wave lengths.

Preface

Core-annular flow is a fascinating physical phenomenon and an interesting topic of research. I am intrigued by nature's ability to arrange itself in such a way that it reaches the most efficient configuration. Core-annular flow has been introduced to me by prof. dr. ir. Gijs Ooms. His vast experience on the topic and guidance of the project is very much appreciated. I also would like to thank prof. dr. Ruud Henkes for his supervision of the project. Discussions on the results and new ideas combined with detailed feedback have steered the project towards the present result. I thank dr. ir. Bas van Oudheusden for his involvement and asking the critical questions when necessary. I would like to thank dr. ir. Alexander van Zuijlen for complementing the graduation committee.

The results of this research will be presented at the 14^{th} *International Conference of Multiphase Flow in Industrial Plant*, for which a conference paper has been written in collaboration with prof. Ooms and prof. Henkes. This shows trust in the integrity of my work, which gave me the motivation in the final stage of the project. Furthermore, it was prof. Henkes' idea to present the results at the *Burgers Symposium* in May 2017. This opportunity was an unforgettable experience.

I want to express my gratitude to everyone who has helped me during the project. In particular: Visiting PhD candidate Gianluca Losi, for his help with the set-up and the start of the development of a new sensor. Ben Norder, of the faculty for Applied Sciences, for the viscosity measurements. Dr. Menno van Dijk, of the Shell Laboratory in Amsterdam, for interfacial tension measurements. The support staff of Fluid Dynamics: Jasper Ruijgrok, Edwin Overmars and Jan Graafland. The P&E lab supervisors: Jaap van Raamt and Michel van den Brink. And Carsten Sanders, for his assistance during the experiments.

Coffee breaks and discussions with my fellow students at the Masters' room, in particular Maarten Klapwijk, Rhoheth Radhakrishnan and Carsten Sanders, have been a welcome addition to the graduation project.

Last, but certainly not least, I want to thank my family for their love and support during my study. And my dearest Charlotte, thank you.

Erik van Duin
Delft, August 2017

Table of Contents

List of Figures

List of Tables

Chapter 1

Introduction

Multiphase flow is an interesting topic from a fundamental research perspective as well as for industry application. The term multiphase flow is used to refer to any flow consisting of two or more immiscible phases. Examples are gas-liquid flow, liquid-liquid flow and gas-liquid-solid flow. Alternatively, one can use the specific names of the different phases to identify the type of multiphase flow, such as water-air flow, oil-gas flow, oil-water flow or oil-water-gas flow.

Two-phase liquid-liquid flow consists of two clear distinct immiscible liquid phases. If one phase dissolves into the other, the flow would be a single phase flow. An oil-water flow is a clear example of liquid-liquid two-phase flow and is studied in detail in known literature, see for example the books of Joseph and Renardy [1, 2].

Depending on the flow conditions different flow regimes can occur. A schematic impression of all observed flow regimes is presented in Brauner [3] and is given in figure 1.1. Here the black and white phases represent oil and water, respectively. For example, stratified flow is represented in schematic (a) and oil-in-water and water-in-oil emulsions are given in schematics (i) and (j). It is also possible that a core of one fluid forms surrounded by an annulus of the other, as shown in schematics (k) and (l). This type of liquid-liquid two-phase flow is called core-annular flow.

According to Joseph and Renardy [2] it is a "gift of nature that the fluid with low viscosity migrates to the regions of high shear". Core-annular flow is the result of this *gift of nature*, where the core consist of the high viscosity fluid and the low viscosity fluid is situated in the annulus, see figure 1.1 (k). In this flow regime the annulus acts as a lubrication layer and this enables the very efficient transport of very viscous liquids.

With the depletion of light crude oil in reservoirs, the petrochemical industry has raised their interest in heavy crude oils. These oils have a (much) larger viscosity and thus flow less easily. Methods to enhance the transportation require further research. Traditionally, heavy crude oils are heated up or diluted to reduce the viscosity. An alternative is using core-annular flow for transportation, where the very viscous oil is lubricated by a layer of water.

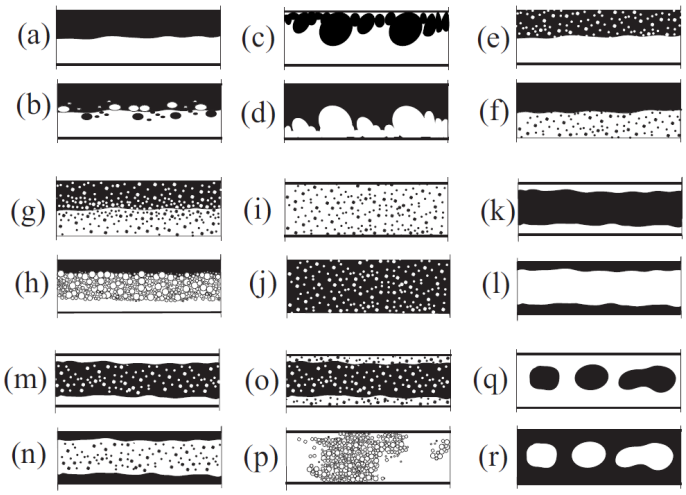

Figure 1.1: Different flow patterns for liquid-liquid two-phase flow [3]. The black phase is oil and the white phase is water.

Figure 1.2 provides an overview of the different methods [4], where the pressure drop is given as function of the volumetric flow rate. The pressure drop balances the friction between the pipe wall and the fluid at a certain flow rate and this pressure drop is used to determine the pumping power required for transportation through a pipeline. The curves at the top of the figure display the pressure drop for two heavy crude oils, with a viscosity of 80,000 cSt and 11,200 cSt respectively. As a reference, the pressure drop for water flow only is included.

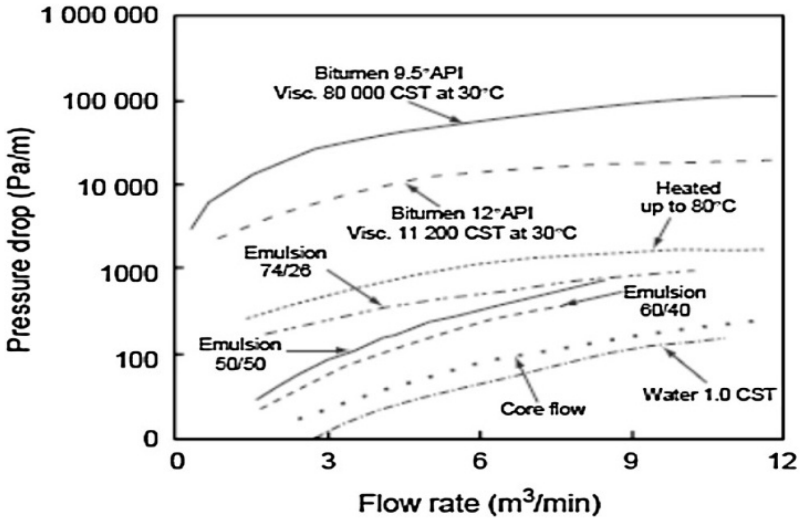

Figure 1.2: Pressure drop as function of the flow rate for various ways of transporting heavy oils in the Venezuela oil industry [4]. The pressure drop for water (1 cSt) only is included for reference.

Heating up the oil decreases the viscosity and thus the pressure drop. The curves indicated with *emulsion* correspond to a dilution of the heavy crude and the pressure drop is reduced more efficiently than for heating. The dotted line, indicated with *core flow*, corresponds to core-annular flow. As observed in this graph, this is by far the most efficient way to transport very viscous fluids through pipelines.

1.1 Research objective

From the introduction above it can be concluded that core-annular flow can be a very suitable candidate for the transportation of very viscous fluids. Before large scale implementation of this technique further research is required.

This research project has the aim to determine the influence of the oil viscosity on core-annular flow. This is done through pressure drop measurements and visualisation with a high-speed camera. In the known literature, a systematic experimental study on the core viscosity has not been found.

1.2 Outline of the report

The report is the result of an experimental study on the influence of the viscosity on core-annular flow. Chapter 2 starts with theory on multiphase flow and core-annular flow in particular. The fluid properties play an important role and are elaborated on in chapter 3. The used experimental set-up and the modifications made are described in the following chapter. The set of experimental conditions and the explanation of a typical experiment are the topic of chapter 5. The results for the pressure drop measurements are presented in chapter 6, whereas in chapter 7 the acquired images of core-annular flow are discussed. The report is ended with the main conclusions and recommendations for further research and improvements of the set-up.

To extend the work, two major problems were encountered during experimentation which are described in appendix B.

Chapter 2

Theoretical Background

In this chapter, an overview of relevant theory of core-annular flow is presented. It starts with basic definitions on multiphase flow and the studied geometry. Dimensionless number concerning the problem are presented, followed by the levitation mechanism. Two models to predict the pressure drop are discussed and this chapter is concluded with a short comment on previous experimental work.

2.1 Basic concepts and definitions

The concepts and definitions presented in this section are widely used for the description of multiphase flows, see for example the PhD thesis by Shi [5] and Bratland's *Pipe flow 2: Multi-phase flow assurance* [6].

2.1.1 Geometry

Multiphase pipe flow describes the simultaneous flow of different phases in the same pipe. It is clear that the different phases can not occupy the same volume at the same time. A cross section of the pipe is given in figure 2.1, where a perfect cylindrical core is located concentrically in the pipe. This configuration is often referred to as *perfect core-annular flow*. In the figure the parameters of the water and oil phases are included. The inner radius of the pipe is denoted by R, and the diameter of the inner pipe is $D = 2R$. The radius of the core is denoted by R_c and the thickness of the annulus is given by t_a.

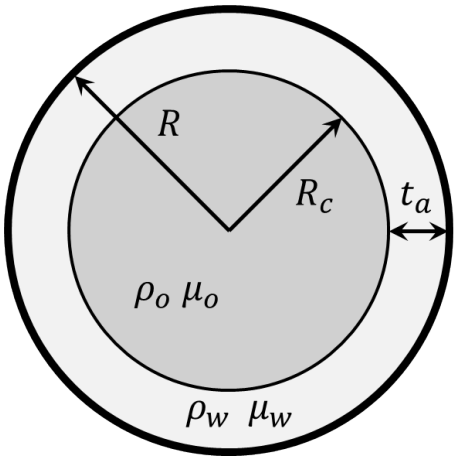

Figure 2.1: Schematic representation of a cross section of perfect core-annular flow.

2.1.2 Phase hold-up

Taking a cross section of the pipe, the area occupied by one phase is the phase hold-up. By dividing the hold-up with the cross sectional area, the hold-up fraction is found. For every phase a hold-up fraction is defined and will be denoted by H_i, where i indicates the phase of interest. It is easily seen that the sum of all hold-up fractions equals 1. For oil-water two-phase flow the hold-up fractions are given as:

$$H_w = \frac{A_w}{A} \tag{2.1a}$$

$$H_o = \frac{A_o}{A} = 1 - H_w \tag{2.1b}$$

The subscripts o and w stand for oil and water, respectively, which will be used in this report to indicate the two phases.

2.1.3 Watercut

For oil-water two-phase flow, the phase input volumetric fraction of water is often named as the watercut. The watercut, C_w, is defined as the ratio of the water volumetric flow rate, Q_w, and the total volumetric flow rate of oil and water, $Q_o + Q_w$. In a similar way the oilcut, C_o, can be defined.

$$C_w = \frac{Q_w}{Q_o + Q_w} \tag{2.2a}$$

$$C_o = \frac{Q_o}{Q_o + Q_w} = 1 - C_w \tag{2.2b}$$

2.1.4 Hold-up ratio

It is common in core-annular flow studies to define the hold-up rate through:

$$h = \frac{A_w/A_o}{Q_w/Q_o} \tag{2.3}$$

When the hold-up ratio is larger than 1, this means that the water is accumulating. For a hold-up ratio smaller than 1, oil is accumulating.

It is observed, for example by Arney et al. [7], that for core-annular flow the water hold-up fraction is consistently larger than the watercut. This means that water is being held back. The slower water velocity must lead to a thicker annulus in order to satisfy the volumetric flow rates. The core diameter is thus reduced and the water hold-up is increased.

Arney et al. [7] also state that the core diameter is in general determined by a balance of the hydrodynamic forces, interfacial tension and internal stresses. A Newtonian fluid cannot support internal stresses without deformation. Hence, for a given set of fluid properties and flow rates, there exists a unique value for the core diameter which satisfies the force balance.

2.1.5 Hold-up correlation

The actual hold-up is more difficult to measure than the flow rates and varies with space and/or time. To that end, a correlation between the watercut and the water hold-up has been derived by Arney et al. [7]. They used data from twelve different experiments to obtain an empirical relation given as:

$$H_w = C_w \left(1 + 0.35 \left(1 - C_w\right)\right) \tag{2.4}$$

2.1.6 Superficial velocity

For single-phase flow, the instantaneous average velocity is often defined as the volumetric flow rate divided by the cross sectional area of the pipe. It is obvious that for single-phase flow, all area is occupied by the same phase.

In multiphase flow, the volume occupied by a particular phase varies with space and time. The superficial velocity of a phase is a widely used concept in multiphase flow to describe the flow conditions. The superficial velocity is defined as the average velocity if one phase is flowing in the pipe. That is, the volumetric flow rate of phase i divided by the cross section of the pipe results in the superficial velocity, $v_{s,i}$.

The in-situ phase velocity can be computed by dividing the volumetric flow rate by the area occupied by that phase. Taking the definition for the phase hold-up fraction, H_i, the

superficial velocity and actual (average) velocity are related as:

$$v_{s,i} = H_i v_i = \frac{Q_i}{A} \tag{2.5}$$

2.1.7 Mixture velocity and density

The sum of all superficial velocities results in the mixture velocity of the flow. For oil-water two-phase flow, the mixture velocity is:

$$v_{mix} = v_{s,o} + v_{s,w} = \frac{Q_o + Q_w}{A} \tag{2.6}$$

The density of the mixture is computed similarly as the mixture velocity:

$$\rho_{mix} = H_o \rho_o + H_w \rho_w \tag{2.7}$$

2.2 Dimensionless numbers

Five forces acting on core-annular flow are identified and based on a characteristic length scale, L, and velocity, u. These forces are given by:

- Inertial force: $\rho u^2 L^2$
- Pressure force: $\Delta P L^2$
- Gravitational force: $\rho g L^3$
- Viscous force: $\mu u L$
- Surface tension: σL

Dimensionless numbers are derived from the ratio of these forces. Some familiar examples are the Reynolds number, Froude number and Weber number, which can be defined as:

$$Re = \frac{\text{Intertial force}}{\text{Viscous force}} = \frac{\rho u L}{\mu} \tag{2.8}$$

$$Fr = \sqrt{\frac{\text{Intertial force}}{\text{Gravitational force}}} = \frac{u}{\sqrt{gL}} \tag{2.9}$$

$$We = \frac{\text{Intertial force}}{\text{Interfacial tension}} = \frac{\rho u^2 L}{\sigma} \tag{2.10}$$

The Reynolds numbers for the oil and water phases are often expressed in terms of their superficial velocities as:

$$Re_{s,o} = \frac{\rho_o u_{s,o} D}{\mu_o} \tag{2.11}$$

$$Re_{s,w} = \frac{\rho_w u_{s,w} D}{\mu_w} \tag{2.12}$$

The density difference between oil and water results in a buoyancy force on the core. This is a modification of the gravitational force by replacing ρ with $\Delta\rho = \rho_w - \rho_o$. Taking into account the buoyancy force, the Froude number can be rewritten as:

$$Fr = \sqrt{\frac{u^2}{g'L}} \qquad \text{where} \quad g' = \frac{\Delta\rho}{\rho_o} \tag{2.13}$$

Where the Weber number is used for gas-liquid systems, the Eötvös is more suitable for liquid-liquid characterisation. It is given as:

$$Eo = \frac{\Delta\rho g L}{\gamma} \tag{2.14}$$

Note that the surface tension, σ, in the Weber number is replaced by the interfacial tension denoted by γ.

2.3 Levitation mechanism

The oil is often less dense than water. For horizontal core-annular flow, this density difference results in an upward buoyancy force acting on the core. Stable horizontal core-annular flow is thus only possible when the buoyancy force is counterbalanced by hydrodynamic forces exerted by the annulus on the core. The core is levitated in the pipe and the mechanism to keep the core from touching the wall is called the levitation mechanism. There are two theories explaining this mechanism, which both assume that waves on the interface are required.

A levitation mechanism based on hydrodynamic lubrication theory has been proposed by Ooms et al. [8]. This was later refined by Oliemans et al. [9] through taking the turbulent flow behaviour in the annulus into account. The periodic waves on the interface are said to be of a saw tooth shape pattern. It can be regarded as an array of slipper bearings that push the core away from the wall. This type of lubrication mechanism is dominated by the viscous forces.

Joseph et al. [10] proposed a mechanism based on inertia, the *flying core model*, in analogy to their previous work on lift-off of a capsule in pipe flow. A critical lift-off velocity is proportional to the square root of gravity times the density difference, which is an inertial criteria. The flying core model also takes into account the wave smoothing effect due to higher and lower pressure regions discussed in the lubrication model by Ooms et al.

Both models are schematically represented in figure 2.2 and a clear distinction is seen in the pattern of the waves. A numerical study on the levitation mechanism was performed by Ooms et al. [11], where a large viscosity ratio and small density ratio is taken for core-annular flow. The shape of the interface is regarded as a solution of the problem. Both types of interface shapes have been observed. For high Reynolds numbers of the annulus levitation is caused by inertial forces (flying core) and at low Reynolds numbers levitation is due to viscous forces (lubrication). They noted a point of concern on their numerical results: the interface at the bottom in he simulations is smooth, whereas waves are observed in the experiments.

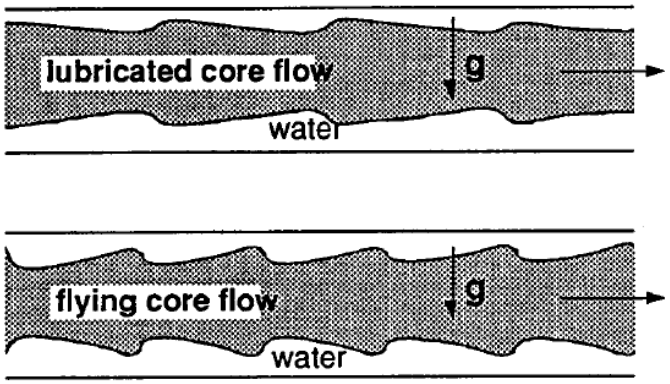

Figure 2.2: Schematic representation of the two levitation models (Image from [10].) Top: Levitation according to the lubrication theory. Bottom: Flying core levitation model.

2.4 Pressure drop models

Two models are studied which predict the pressure drop for core-annular flow consisting of a laminar core flow and a turbulent annulus. Both models will be tested against the measurements.

2.4.1 Model of Brauner

A two-fluid model is used by Brauner [12] to derive relations for the expected pressure drop and core diameter. In this model, the equations of motion are constructed for both phases. The model is applicable when the fluids of interest are clearly separated, like in the stratified and core-annular flow regimes. The system of equations contains more unknown variables than equations and therefore closing relations have to be included. For core-annular flow, the wall friction and interface friction are modelled in order to solve the system of equations.

The final result of the derivation for horizontal flow presented by Brauner consists of four relations: the Martinelli parameter, X^2, the slip factor at the interface, c_i, the in-situ core hold-up, $\tilde{D}_c$, and the dimensionless pressure drop, $\frac{d\tilde{P}}{dZ}$. The first three relations are required for the final expression of the pressure drop.

The Martinelli parameter expresses the phase fraction of a flow. For a laminar core – turbulent annulus, Brauner expresses this number as:

$$X^2 = \frac{0.046}{16}\left(\frac{\mu_o}{\mu_w}\right)^{0.2}\left(\frac{\rho_w}{\rho_o}\right)^{0.8}\frac{{Re_{s,o}}^{0.8}}{\tilde{Q}^{1.8}}\,, \tag{2.15}$$

where $Re_{s,o}$ is the Reynolds number based on the superficial oil velocity and $\tilde{Q}$ is the superficial velocity ratio of the core and annulus:

$$\tilde{Q} = \frac{u_{s,o}}{u_{s,w}} = \frac{Q_o}{Q_w}$$

The slip parameter, c_i is estimated to be between 1.15 and 1.2 for the turbulent annulus and laminar core.

The relation for the in-situ core hold-up is expressed as the in-situ water hold-up, $1-\tilde{D}_c^2$, and is given as:

$$1-\tilde{D}_c^2 = \frac{\frac{c_i}{2} - x^2\tilde{Q}{F_i}^{-1} + \frac{c_i}{2}\left[1+4X^2\left(\frac{\tilde{Q}}{c_i}\right)^2{F_i}^{-1}\right]^{0.5}}{c_i + \tilde{Q} - X^2\tilde{Q}{F_i}^{-1}} \tag{2.16}$$

The parameter F_i represents the interfacial friction factor. For liquid-liquid core-annular flow, Brauner has observed that the waves present at the interface are long and smooth in comparison to gas-liquid core-annular flow. The parameter is introduced to account for the possible inclusion of refined models for the interface. Since the annulus is turbulent and the oil and water velocities at the interface are comparable, the interfacial friction factor is set to one, $F_i = 1$.

The relation for the pressure drop of laminar core – turbulent annulus is given in equation (2.17), which is made dimensionless with the pressure drop for the case that only oil is flowing through the pipe with the same volumetric flow rate. This can be interpreted as a reduction factor.

$$\frac{d\tilde{P}}{dZ} = \frac{dP/dz}{(dP/dz)_{s,o}} = \frac{X^2}{\left(1-\tilde{D}_c^2\right)^2} \tag{2.17}$$

Brauner has mentioned that the model underestimates the pressure drop measured in experiments. Possible explanations for the deviation are an increase in wall friction due to:

- Surface irregularities
- Fouling of the pipe wall by a wavy core interface at high oil flow rates
- Eccentric position of the core

Accounting for these effects in the two-fluid model requires modifications in the closure laws used to model the wall and/or interfacial shear stresses.

2.4.2 Model of Bannwart

Bannwart [13] presented a detailed work on the modelling aspects of oil-water core-annular flow and the comparison with experimental data. The article provides design considerations for engineers.

The model of Bannwart uses the approach of a pseudo fluid to predict the pressure drop of core-annular flow. First, the pressure drop is calculated for the annulus fluid flowing alone at the total volumetric flow rate. The calculated pressure drop is than multiplied with a 'two-phase multiplier', which is based on the fluid properties of both phases and the watercut. Both laminar and turbulent flow in the annulus are considered.

Taking into account the density difference, finite viscosity difference and a turbulent flow in the annulus, the expected pressure drop for horizontal core-annular flow can be calculated by:

$$\frac{dP}{dL} = b\left(\frac{\rho_w v_{mix} D}{\mu_w}\right)^{-n} \frac{\rho_w v_{mix}^2}{2D}\left[1-\left(1-\frac{\rho_o}{\rho_w}\right)(1-C_w)\right]^{1-n}\left[1-\left(1-\frac{\mu_w}{\mu_o}\right)(1-C_w)\right]^{-n} \tag{2.18}$$

The assumption is made that the slip ratio at the oil-water interface is 1. The parameters b and n are dependent on the Colebrook friction law and thus depend on the roughness of the pipe. The Blasius set of $b = 0.316$ and $n = 0.25$ is used to compare the model with the pressure drop result reported by Oliemans et al. [9]. The standard deviation is calculated to be $\pm 14\%$, which is, according to Bannwart, "an encouraging result". Other combinations of b and n are dependent on the annular Reynolds number and the relative roughness of the pipe and are provided in [13]-table 3.

2.5 Experimental research

A number of studies have been done on oil-water two-phase flow and in particular on core-annular flow. Review articles by Ghosh et al. [14] and, more recently, by Shi and Yeung [15] present a detailed overview.

A result worth noting is by Grassi et al. [16], where oil-water experiments were preformed with equal pipe diameter as to the set-up used in this research. Their oil has a density of 886 kg/m^3 and a viscosity of 800 Pa·s. Figure 2.3 displays their flow map for horizontal flow. It shows the observed flow pattern as function of the superficial velocities of oil and water.

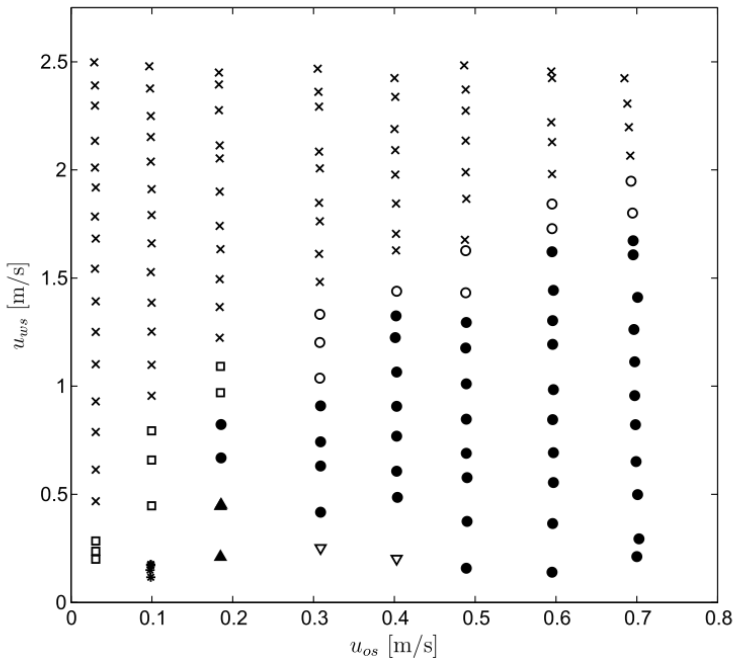

Figure 2.3: Flow map produced by Grassi et al. for zero degree inclination, 21 mm inner pipe diameter and oil viscosity of 800 mPa·s. The superficial velocities of oil and water are given as: u_{os} and u_{ws}. ▲ = stratified flow; × = dispersion of oil in water; • = core-annular flow; □ = plug/slug flow; ▽ = stratified flow and dispersion of oil in water; ○ = core-annular flow and oil in water dispersion; ∗ = oil film at the wall and inner dispersion of oil in water. Image from [16]

Chapter 3

Fluid Properties

Core-annular flow is investigated experimentally by using a very viscous oil and tap water as the fluids in the core and annulus, respectively. The oil density and viscosity and the oil-water interfacial tension play an important role in core-annular flow and have therefore been examined carefully. The oil, *Shell Morlina S2 B 680*, comes with book values of the physical properties. These properties have been measured for this specific batch to ensure the actual properties of the oil used in the experiments. A Dutch version of the technical data sheet of *Shell Morlina S2 B 680* is available on-line by its manufacturer *Royal Dutch Shell* [17]. An English version is included in appendix A.

The viscosity of the oil depends strongly on the temperature and opens the opportunity to vary the core viscosity by changing its temperature. For that purpose the oil density and viscosity are measured as function of temperature. A feasible operation regime to perform experiments is between room temperature (20 °C) and maximum of 60 °C. This has been used as boundaries for the density and viscosity measurements.

The oil is heavily in contact with water during the experiments and afterwards in the separation vessel which can influence its properties. For example, absorption of water by the oil results in an increase in density. Therefore the oil properties are measured using a new and used sample. The new oil sample is taken after one measurement in order to determine its characteristics for further experiments. The used oil sample is taken after completion of all experiments, which is approximately five months later.

An oil sample is taken every month, such that it is possible to trace back when changes in properties could have occurred. As will be discussed in this chapter, it is concluded that the oil properties have not changed significantly during usage and testing of the intermediate samples is thus not necessary.

3.1 Oil density

The density of the oil is measured with an *Anton Paar* density meter available at the Process and Energy department. A small sample of fluid, 2 ml, is required to measure its density with high precision. To take into account reproducibility between various sample, the first four significant numbers are used for analysis. Furthermore, it is also possible to measure the density at various temperatures.

In the core-annular flow experiments, the oil viscosity will be varied by changing its temperature. The oil density as function of the temperature is therefore measured in the same range. The temperature is increased from 15 °C to 65 °C with steps of 5 °C.

Figure 3.1 displays the oil density of the new and used sample as function of the temperature. The density of water is given as a reference. The density decreases with increasing temperature. From this graph it is clear that the oil density is lower than the water density. It is also observed that for both oil samples the density decreases linearly with increasing temperature. The density between the two samples differs at the fourth significant number. The density difference between the new and used sample divided by the new oil sample density is calculated as:

$$\frac{|\rho_{new} - \rho_{used}|}{\rho_{new}} \times 100\%,$$

The average of the value over all measured temperatures is 0.08 percent of the new oil density sample. It can be concluded that this difference is negligible taking into account possible contamination in the measurement device or reproducibility of the test. Since the oil density

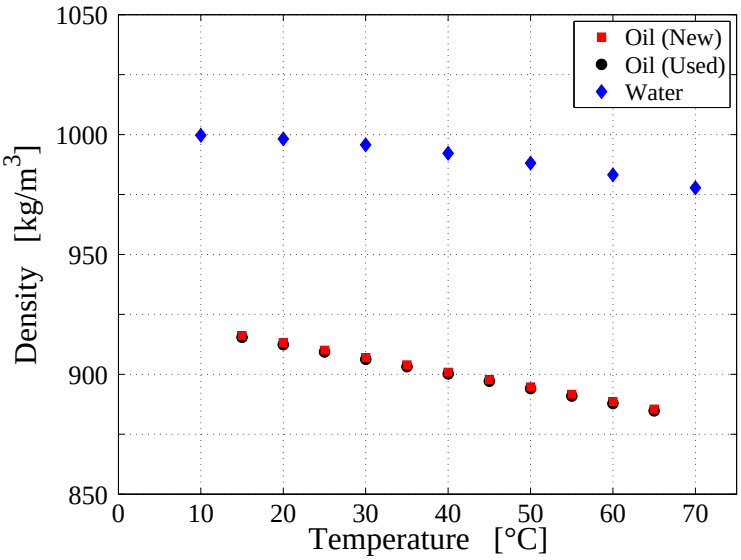

Figure 3.1: Oil density as function of temperature for the new and used oil. The density of water as function of temperature is given as a reference [18].

does not vary over time, it can also be concluded that water is not absorbed by additives present in the oil. If water would have been absorbed, the density should have increased.

The book value of the oil density is 910 kg/m^3 at 15 °C, while 916 kg/m^3 is measured. Although the book value and the measured value differ slightly, it can be concluded that the oil meets the manufacturer specification.

3.2 Oil viscosity

As mentioned in the introduction of this chapter, in the experiments the oil viscosity will be varied by changing its temperature. Therefore it is important to know the oil viscosity as a function of temperature. These measurements have been performed by Ben Norder of the faculty of applied sciences of TU Delft. A rheometer of *TA Instruments*, type AR-G2 is used. A Taylor-Couette flow geometry is used, in which the inner cylinder rotates with a prescribed velocity and the outer cylinder is stationary. The shear rate generated by the rotating cylinder induces a shear stress on the fluid. The dynamic viscosity is the slope of the shear stress as function of the shear rate. A thermal bath around the measurement section enables testing the fluid at different temperatures.

The rheometer is programmed to evaluate the sample at pre-set shear rates for one temperature. When an equilibrium state is reached in three measurement time intervals, the relevant data are automatically stored. The temperature is varied from 20 °C to 60 °C with intervals of 5 °C. To capture a possible hysteresis effect in the viscosity results, the oil temperature

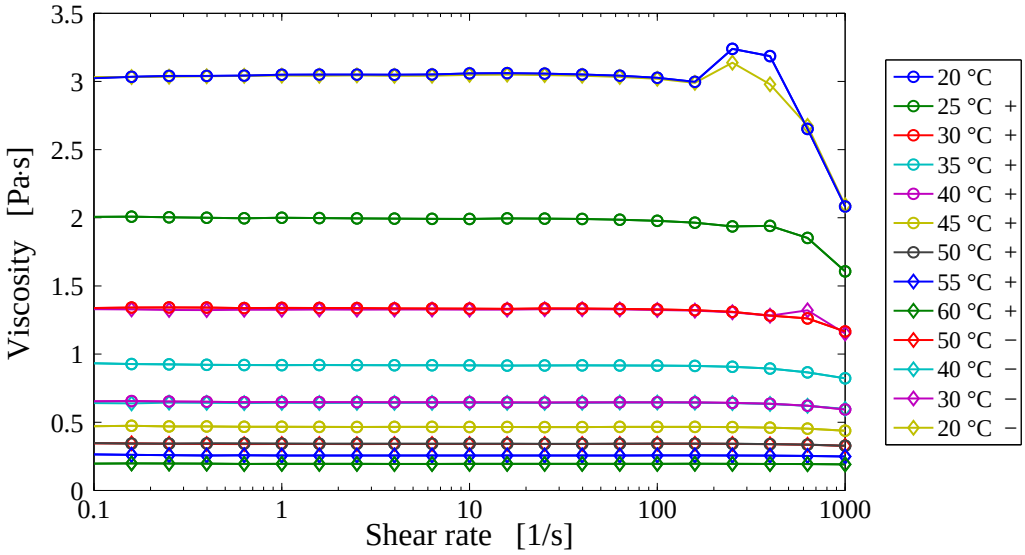

Figure 3.2: Measurement series to determine the dynamic viscosity of the new oil sample at different temperatures. In the legend, the temperature is given followed by a plus or minus sign which indicates increasing or decreasing temperature with respect to the previous measurement.

is also decreased from 60 °C to 20 °C with steps of 10 °C. Sufficient time is incorperated in between the measurement series to obtain thermal equilibrium.

The results of the viscosity as function of the shear rate is presented in figure 3.2, where the shear rate is varied logarithmically from 0.1 s^{-1} to 1000 s^{-1}. At high shear rate, i.e. above 100 s^{-1}, the viscosity starts to deviate from the horizontal line that one would expect to hold. This is most clearly observed for the 20 °C measurement series. The decrease in viscosity is explained by the oil creeping up the inner rotating cylinder. Also a Taylor vortex could have been formed in the fluid due to the high shear rate which leads to a larger observed viscosity. At low shear rates, it is possible that velocity profile is not uniformly settled yet and small deviations in viscosity are observed in the data. This is not evidently present in the graph.

Based on the observations, the oil viscosity at a given temperature is calculated as the average of the shear rate in the closed interval from 0.3981 s^{-1} to 100 s^{-1}. Table 3.1 gives an overview of the averaged viscosity for the increasing and decreasing curves. A small deviation in the viscosity of less than 1 percent is seen between the increasing and decreasing temperature measurement. It is more likely that the temperature has not fully reached an equilibrium state rather than that a hysteresis effect is taking place.

The same procedure has been performed for the used oil sample. The result of the viscosity as function of temperature for the new and used oil sample are presented in figure 3.3. Both curves overlap and it can thus be concluded that the oil viscosity has not changed during usage.

In further analysis of core-annular flow the viscosity of the new sample is used. This holds also for the calculation of the kinematic viscosity in the next section.

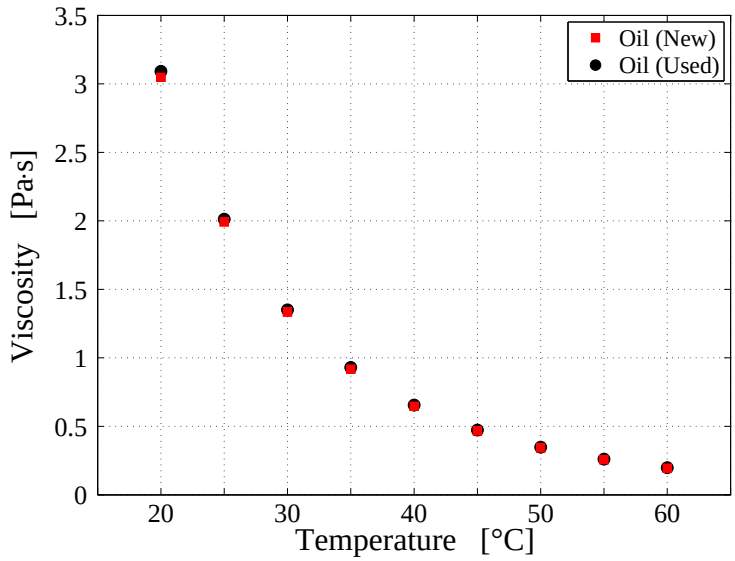

Figure 3.3: Viscosity as function of temperature for the new and used oil sample.

Table 3.1: Viscosity of the new oil sample for different temperatures. The last column indicates the difference between the increasing and decreasing measurement with respect to the average of the two values.

Temperature [°C]	Viscosity [Pa·s]		Difference
	Increasing	Decreasing	
20	3,0483	3,0408	0.25%
25	1,9931		
30	1,3350	1,3263	0.65%
35	0,9182		
40	0,6468	0,6426	0.64%
45	0,4660		
50	0,3426	0,3406	0.59%
55	0,2565		
60	0,1949		

3.2.1 Kinematic viscosity

The oil kinematic viscosity, ν_o, is calculated using the measurements for the oil density, ρ_o, and dynamic viscosity, μ_o, as:

$$\nu_o = \frac{\mu_o}{\rho_o}\,, \tag{3.1}$$

The unit of the kinematic viscosity is m^2/s. In the petrochemical industry this quantity is often expressed in centi-Stokes (cSt), where 1 cSt = 1 mm^2/s = 10^{-6} m^2/s.

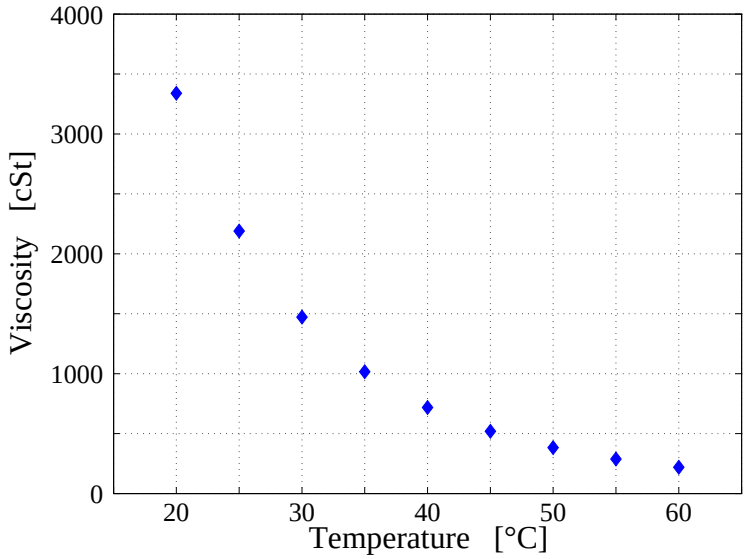

Figure 3.4: Oil kinematic viscosity as function of temperature.

In figure 3.4 the kinematic viscosity as function of temperature is presented. As was also observed for the dynamic viscosity, the kinematic viscosity decreases exponentially with increasing temperature.

Comparison of the book value and measured value of the kinematic visocisty at 40 °C yields 680 cSt and 718 cSt, respectively. Our batch of *Morlina S2 B 680* is thus slightly more viscous than specified and could be named, more appropriately, as *Morlina S2 B 718*.

3.3 Interfacial tension

The surface tension of a liquid is described as its elastic tendency to acquire the least surface area possible. For liquid-gas interfaces, the liquid molecules have a greater attraction towards other liquid molecules than to the gas phase. This results in a net force on the interface directed into the liquid phase and behaves as if the liquid is covered by an elastic membrane. In the case of two immiscible liquids, the surface tension between the two phases is referred to as the interfacial tension.

The interfacial tension between oil and water is measured using a *Krüss* ring tensiometer [19] at Shell Amsterdam under supervision of dr. Menno van Dijk, who is a colleague of Ruud Henkes.

The working principle of a ring tensiometer to measure the surface tension was first described in 1919 by Lecomte Du Noüy and consists of a horizontally suspended platinum ring which is immersed in a liquid and then lifted out again. The maximum force required to pull the ring through the interface is measured. By dividing the maximum force acting on the ring by the wetted area of the ring, that is covered by the inner and outer circumferences of the ring, the surface tension of the liquid is obtained.

Harkins and Jordan [20] noticed that the shape of the interface on the inner and outer part of the ring differs. Furhtermore, the weight of the liquid film raised by the ring produces a force on the ring. They systematically investigated the technique and derived a semi-empirical correction factor based on the ring dimensions and the density difference between the liquid and air.

In 1941, Zuidema and Waters [21] developed this technique further to measure the interfacial tension between two liquids. The density difference between the two phases is smaller than for liquid-air. Now an extra force is acting on the volume of liquid lifted by the ring by the upper liquid and needs to be corrected for, see equation 3.3.

The Krüss ring tensiometer is calibrated for the used ring and displays the measured interfacial tension, γ^*. The actual interfacial tension, γ, is calculated as:

$$\gamma = \gamma^* \cdot f = \frac{F_{ring}}{4\pi R^2} \cdot f \,, \tag{3.2}$$

where f is the correction factor determined by Zuidema and Waters [21]. On the right side,

the relation is given that is used to calculated the surface/interfacial tension from the force acting on the ring, F_{ring}, and the total wetted area of the ring, $4\pi R^2$.

In the manual is mentioned that the measured interfacial tension first needs to be multiplied by a factor 1.07, which is posed as a *Krüss correction factor*. Afterwards the correction factor, f, is determined as:

$$f = a + \sqrt{\frac{4b}{\pi R^2}\frac{\gamma^*}{\Delta\rho} + C}\,, \tag{3.3}$$

where R is the radius of the ring (in centimeter), $\Delta\rho$ is the density difference between the two liquids (in gram per cubic centimeter), a and b are constants ($a = 0.725$ and $b = 9.075\times10^{-4}$) and C is a parameter based on the geometry of the ring.

$$C = 0.04534 - \frac{1.679}{R/r}$$

The ratio $\frac{R}{r}$ is the radius of the ring divided by the radius of wire.The used ring has a radius of 1 cm and the ratio $\frac{R}{r}$ is 51.6.

The interfacial tension between oil and tap water from the set-up is measured by the following steps:

- Fill the container with tap water.
- Clean the ring using a burner to red heat.
- Reset the scale to zero (exclude the weight of the ring itself).
- Immerse the ring in water.
- Gently pour oil on top of the water.
- Let the interface settle for five minutes
- Carefully pull the ring through the interface.
- Clean the system and repeat the measurement.

The maximum force on the ring is based on a quasi-equilibrium state of the forces in the system. Since the oil is very viscous, it reacts slowly to the movement of the ring. It is therefore important to raise the ring through the interface by small increments and let the force balance return to equilibrium. Too fast movement will result in an overshoot in the maximum observed force and thus an error in the interfacial tension.

The interfacial tensions between the new oil sample and tap water and the used oil sample and water are measured three times each. The results of the measured and corrected measurements are displayed in table 3.2. The average of the true interfacial tensions are listed in the last column.

The interfacial tension for the new and used oil sample differs by factor 1.22. It would be expected that the interfacial tension remains constant or decreases over time. An explanation for the increasing value is hard to give. This technique is susceptible for measurement error, e.g. raising the ring too fastly results in an overestimation of the interfacial tension. A combination of different techniques for interfacial tension measurements can give more clarity on the difference.

Table 3.2: Measured and corrected interfacial tension (IFT) of the new and used *Morlina S2 B 680* oil with tap water at 20 °C.

Oil Sample	Measured IFT [mN/m]	Corrected IFT [mN/m]	Averaged, true IFT [mN/m]
New	13.7	14.7	13.8
	12.6	13.4	
	12.5	13.3	
Used	16.1	17.6	16.9
	14.9	16.2	
	15.5	16.9	

The interfacial tension is only measured at 20 °C. At the Shell Laboratory it was possible to vary the temperature of the total sample. Since the available time was limited and the warming process would take quite some time per measurement these measurements have not been performed. The literature suggests that the temperature has a small effect on the interfacial tension in the region of interest between 20 °C and 50 °C. A study by Peters and Arabali [22] shows a slight increase of the oil-water interfacial tension for a comparable oil, where Flock et al. [23] find a small decrease in the interfacial tension between heavy crude oils and water. It must be noted that both studies use an inverted pendant drop method to measure the interfacial tension.

For the remainder of this thesis, the interfacial tension for the new oil sample is used and it is assumed to remain constant for the applied temperature range.

3.4 Fluid properties of Shell Morlina S2 B 680

It is concluded from the measurements that the fluid properties of the *Morlina S2 B 680* oil are stable over time. The density and viscosity have not changed significantly. The interfacial tension shows a slight increase, which is assumed to be beneficial for the stability of core-annular flow.

Table 3.3 gives an overview of all fluid properties based on the new oil sample. As will be discussed in chapter 5, a feasible temperature domain for the viscosity is from room temperature to maximum 50 °C. This domain is thus used in the overview in the table.

Table 3.3: Overview of the oil properties of *Morlina S2 B680* from 20 °C to 50 °C.

Property	Symbol	Range	
Density	ρ_o	913.1 – 894.7	kg/m^3
Dyn. viscosity	μ_o	3.048 – 0.3426	Pa s
Kin. viscosity	ν_o	3339 – 383.0	cSt
Interfacial tension	γ	13.8	mN/m

3.5 Water properties

The lubrication fluid in the annulus is tap water and is measured to be around 15 °C. Just as the oil properties, the water density and viscosity also depend on the temperature, but not as heavily as the oil does. For further analysis, the water properties at 15 °C are used, as taken from [18], and they are listed in table 3.4.

Table 3.4: Water properties at 15 °C [18].

Property	Symbol	Value	
Density	ρ_w	999.1	kg/m^3
Dyn. viscosity	μ_w	1.1375 $\times 10^{-3}$	Pa s
Kinematic viscosity	ν_w	1.1386	cSt

Chapter 4

Experimental Set-up

An experimental set-up is made to study core-annular flow of a very viscous oil and tap water. The set-up has been used prior to this research and is already calibrated and refined. The calibration of the various components has been done by the previous student and will be referred to when appropriate.

In this chapter the structure of the set-up will be described, followed by the data acquisition system and sensors. Afterwards the modifications made to the set-up are described. To conclude, a typical procedure of an experiment is given.

4.1 Lay-out of the set-up

Schematic overviews of front and back of the experimental set-up are presented in figures 4.1 and 4.2. In the front part the flow loop is located in which the experiments are done and it is described in the first part of this section. The second part explains the various components located at the back of the set-up.

4.1.1 Front side

The flow loop on the front side is made of PVC and has a length of approximately 7.5 meters with an inner diameter of 21 mm. In downstream order, the flow loop consists of the following parts, where items with an asterisk will be described in more detail below.

- Divider*.
- 2 m straight section.

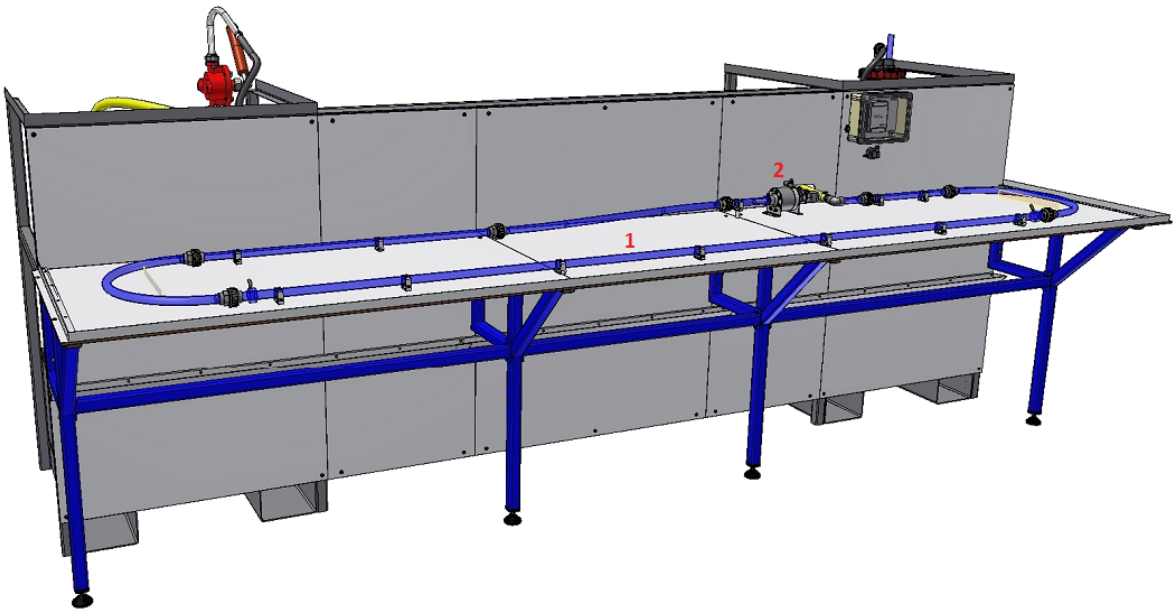

Figure 4.1: Schematic overview of the front side of the experimental set-up. Item 1: Measurement pipe of the flow loop. Item 2: Divider.

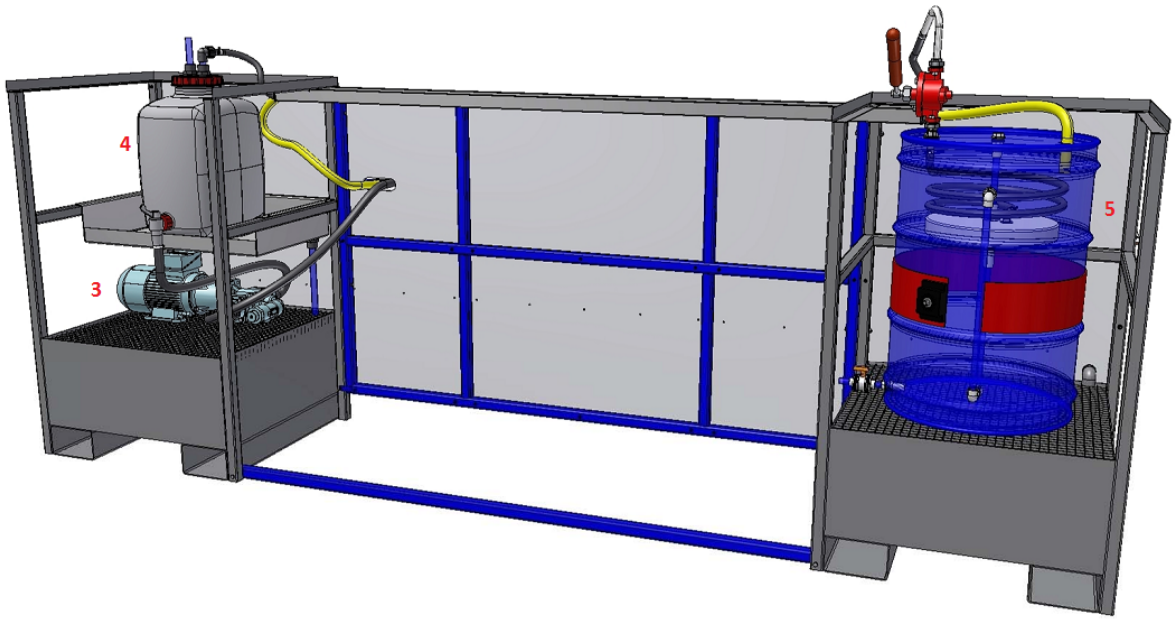

Figure 4.2: Schematic overview of the back side of the experimental set-up. Item 3: Oil pump. Item 4: Oil container with a copper coil inside to heat up the oil. Item 5: Separation vessel for oil and water.

- 180° bend with a radius of 0.25 m.
- 3 m test section*.
- 180° bend with a radius of 0.25 m.
- 0.25 m straight section.
- 4 m hose connecting the flow loop to the separation vessel.

The pipe sections are connected by re-attachable links, such that a pipe-on-pipe connection is created. Also for cleaning purposes it is favourable to have re-attachable links. The flow loop is supported by height adjustable mounts for horizontal alignment.

Divider

The flow starts at the inlet device called the divider. This device imposes the core-annular flow pattern already at the start of the flow loop. The divider has an inner pipe which is concentrically placed within an outer pipe. Oil enters the flow loop via the inner pipe and water via the annular space between the two pipes. A schematic of the internal structure is given in figure 4.3, where the two fluids are indicated.

Measurement pipe

A new, 3 metre measurement pipe, made of transparently casted PMMA, is installed prior to the experiment and is described in more detail in section 4.4. Two pressure points are used to measure the pressure drop over a metre pipe length. They are flush mounted with the pipe wall and are located at the bottom of the pipe to prevent fouling. Furthermore, they are located sufficiently far from the bends.

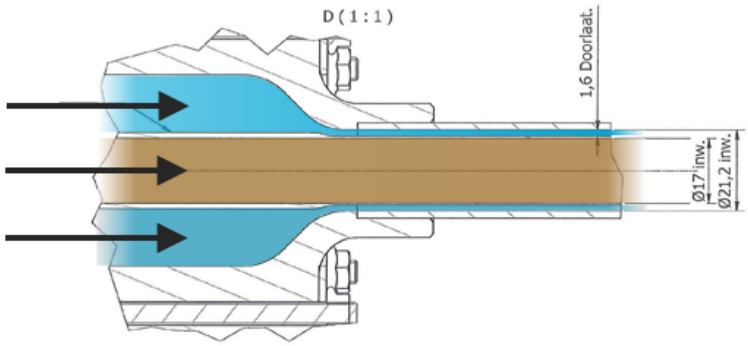

Figure 4.3: Schematic of the internal structure of the divider. The oil flow is indicated in the centre by brown and water for the formation of the annulus is indicated in blue. The arrows indicate the flow direction.

A redesigned imaging section is located in between the two pressure taps to obtain clear optical access. A mirror is used to capture a front and top view simultaneously. A detailed description of this part is given in section 4.6

4.1.2 Back side

The main components on the back side of the set-up are described below.

Separation vessel and dump vessel

After an experiment the flow is directed to the separation vessel where the oil-water mixture is separated due to the density difference between the two liquids. After separation the oil can be reused in further experiments. Inside the 209 litre vessel a floater is placed to pump off the lighter oil. A drain valve at the bottom of the separation vessel is used to dispose the water to a 1000 litre dump vessel (not present in the schematic). Since the water has been in contact with oil it needs to be disposed appropriately.

The separation time is estimated by means of a force balance for a spherical water droplet with an estimated diameter, $2R_d$, in the oil phase. The downwards force, $F_{g,\Delta\rho}$, due to the density difference is in equilibrium with the drag force, $F_{d,sphere}$, as if it is a solid sphere. The terminal velocity, U_t, of the sphere is determined as:

$$\begin{aligned} F_{g,\Delta\rho} &= F_{d,sphere} \\ \left(\frac{4}{3}\pi {R_d}^3\right)\Delta\rho\, g &= 6\pi R_d\, \mu_o\, U_t \\ U_t &= \frac{2}{9}\,\frac{\Delta\rho\, {R_d}^2\, g}{\mu_o} \end{aligned}$$

The height of the oil layer in the separation vessel is approximately 27 cm. Oil drops with a diameter of 0.47 mm and larger are separated within 22 hours, which is experienced to give sufficient segregation.

Oil storage tank and heating system

A small electric gear pump is used to transport the oil from the separation vessel to the oil storage container. From the oil storage container, the oil can be used to perform experiments.

Inside the oil container a copper coil pipe is located, which is connected to a heating device. Hot water is pumped through the copper coil to heat up the oil to the desired temperature. An external thermometer is connected to the heating device. It was noted that the temperature displayed on the heating device is higher than the one measured at the inlet device.

Heating up the oil takes some time since the thermal conductivity is small. It can take about 2 hours to heat up the oil to 50 °C.

Oil pump

An heavy duty gear pump is used to generate the oil flow for the experiments. A three–way valve is connected to the outlet of the pump, meant to direct the oil flow to the experiment or to recirculate the oil in the oil container. This is benificial when heating up the oil. The pump is operated on the front side of the set-up.

The pump produces heat, which was assumed to be insignificant since it is only active for one and a half minute during the experiments. However, in the temperature profile an increase of more than one degree Celsius was observed. This is considerably reduced by recirculating the oil for one minute prior to an experiment.

Rinsing system

Not present in figure 4.2 is a dedicated rising system that consists of a boiler to provide warm water, a separate water container and a pump. By using an additional pump higher flow rates can be obtained than by using the tap. Proper rinsing of the system is necessary to remove all oil residue and thus to maintain similar flow conditions at each experiment. The water used for rinsing is disposed to the 1000 litre dump vessel.

4.1.3 Data acquisition

LabVIEW by *National Instruments Corporation* is used to collect, process and save the data from different sensors installed in the setup. The sensors, combined with their calibration, will be discussed hereafter.

The analogue signals are digitized by a data acquisition device, DAQ, which is connected to a computer. The sensors are sampled at a frequency of 100 Hz and are stored automatically into a single text file with `.lvm` extension. Furthermore, relevant information of the experiment is displayed real-time by the program.

Due to electronic noise generated by the oil pump, the analogue signals are sampled in differential form at the DAQ. This means that two channels are used to transport one signal, which reduces the electronic noise.

4.2 Sensors and calibration

A total of four measurement sensors are built in the experimental set-up to gather data of core-annular flow. The oil and water volumetric flow rates and the oil temperature will be discussed below. The pressure drop is also recorded digitally. This is a new feature in the set-up and is described in detail in section 4.5. Calibration of the first three sensors are done by Ingen-Housz and are described in his master thesis [24]. The safety sensors are briefly discussed in section 4.2.4.

4.2.1 Oil flow rate

The oil pump is frequency driven meaning that the frequency of the power supply is adjusted in order to control the flow rate produced by the pump. Up to an oil flow rate of approximately 0.6 l/s the flow rate is linearly dependent on the frequency. The frequency of the pump is calibrated to the oil flow rate with an uncertainty of within 0.5%, see the thesis of Ingen Housz [24]. The linear calibration is incorporated in the LabVIEW operation program and the converted oil flow rate is stored in the log-file.

4.2.2 Oil temperature

Prior to the divider the oil temperature is measured. From the temperature, the actual oil viscosity entering the flow loop can be derived, as measured in chapter 3.2. The temperature is measured as an analogue signal.

4.2.3 Water flow rate

A *Biotech* turbine flow rate meter is used to measure the volumetric water flow rate. It is placed in between the tap connection and the divider, where an adjustable valve is used to set the water flow rate.

The digital sensor measures 1150 pulses per litre and thus corresponds to $8.7 \times 10^{-}4$ litre per pulse. Every second the amount of pulses is sampled and is converted to the volumetric flow rate. A calibration check performed by Ingen Housz [24] shows that the actual water flow rate deviates up to 4% from the measured flow rate.

A maximum water flow rate of 0.11 l/s is achievable in the current configuration of connection tubes, water flow meter and divider.

4.2.4 Safety sensors

Besides data sensors, several operation and safety sensors are incorporated in the set-up, which are connected to the DAQ board and displayed in the LabVIEW environment as indicator lights.

1. Over-pressure sensor oil pump:
   In case of an severe obstruction in the flow loop, the oil pump needs to shut down automatically. Since it is a gear pump, it keeps pumping and the pressure in the flow loop increases. To avoid loss of containment and/or injury the oil pressure prior to the divider is limited to 5 bar maximum. The over-pressure sensor is directly linked to the pump and does not need the LabVIEW program to be activated. The indicator in LabVIEW is just for monitoring.

2. Minimum fluid level sensor oil container:
   To prevent the oil pump from running dry, a sensor is placed near the bottom of the oil storage tank. When the fluid level is too low, the pump is automatically shut off to prevent damage. Again, this sensor is connected to the pump directly and the indicator in LabVIEW is monitoring of the experiment.

3. Maximum level indicator separation vessel:
   To prevent the separation vessel from overfilling, a sensor is placed below the real maximum. When the vessel becomes too full the indicator in LabVIEW turns red. In this case the flow needs to be stopped accordingly to prevent overflowing.

4. Maximum fluid level indicator dump barrel:
   The 1000 litre dump vessel is located on the ground floor and is not easily checked from the set-up. When the indicator turns red, dumping of waste water needs to be stopped immediately.

4.3 Modifications

During the project the set-up is modified. Some of these points will be briefly discussed below, where others require a more detailed description in a separate section afterwards.

- New measurement pipe and pressure points.
- Implementation of an electronic pressure sensor.
- Visualisation section.
- Changed oil in the set-up.
- Safety assessment sheet
- Heating system to control the oil temperature.
- Improvements of the rinsing system

During the coarse of this study new safety regulations were implemented in the laboratory of Process & Energy where the set-up is located. One of these changes requires a safety assessment sheet at each set-up. This has of course been made on request of the lab supervisor and is now mounted at the set-up.

The heating system to increase the oil temperature was installed prior to the start of this project. A *Julabo* heating circulator with external temperature sensor is used. The device heats up water which is circulated trough a copper coil inside the oil storage container and by heat exchange the oil is warmed up. The external temperature sensor is used to check the oil temperature. The internal temperature, displayed on the device, is the temperature of water inside the heater.

It is noted that the oil temperature displayed by the heating device and the oil temperature measured at the experiments differ. The oil temperature before the divider is lower by approximately 0.5 to 1.5 °C depending on the final temperature.

Some improvements on the rinsing system are implemented to increase its functionality and ease of use. The water container has been replaced and the system is now leak free.

When the rinsing system is connected it is now possible to rinse in closed or open loop by means of a three-way valve. In the open loop circuit mode, the warm water (with or without detergent) is pumped through the flow loop and is disposed after one circulation. In closed circuit, the rinsing fluid can be recirculated for a longer time to clean the flow loop more thoroughly. All rinsing water is disposed in the dump barrel.

4.4 New measurement pipe

A new, 3.05 m long measurement pipe is installed in the set-up. It is made of transparent cast PMMA and, in general, this material has a lower wall roughness than PVC. It is also more transparent when comparing it to other pipe sections of the flow loop. This will improve the quality of the visualisation study.

In total three pressure holes are made, all spaced 1 m apart. The most upstream pressure hole is approximately 0.7 m downstream of the first 180° bend and will not be used for the experiments. The most downstream pressure hole is still sufficiently far away from the downstream 180° bend.

The new pressure connections, as designed by Carsten Sanders, are glued to the pipe, see figure 4.4. It is now possible to observe the inside of the pipe where the pressure hole is located and it becomes easier to detect possible fouling at or around the pressure hole. A small diameter pipe can be shifted up or down and then tightened to ensure a flush connection between the pressure tube and the pipe wall. Additional tubes are used to connect the pressure point to the differential pressure transducer.

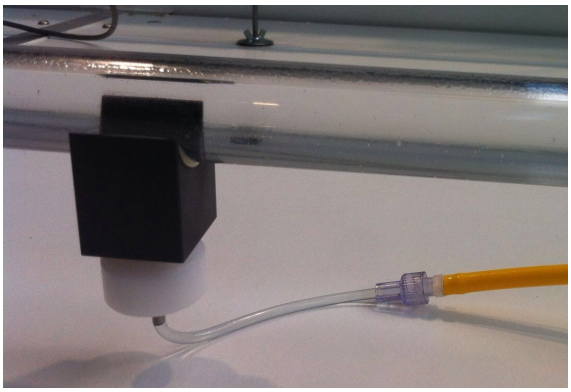

Figure 4.4: Photograph of the newly designed pressure hole connector.

One disadvantage of the new measurement pipe is the glued connection. The maximum length of a pipe piece is 2.05 m and therefore 2 pipes are glued together. After an experiment, when the oil flow is stopped, it happens that the roughness created due to the connection trips the oil tail and fouling occurs. Intense rinsing does not remove the oil, but smears it out downstream. A piece of sponge on a rope in combination with water and detergent is used to clean the measurement pipe.

4.5 Electronic pressure sensor

One of the main improvements of the set-up is the implementation of an electronic pressure sensor instead of an inverted U-tube to measure the pressure drop. This has the advantage of a more accurate pressure measurement when properly calibrated. Furthermore, the signal is recorded and stored using the LabVIEW operation program.

4.5.1 Validyne differential pressure transducer

A differential pressure transducer from *Validyne Engineering*, model *DP15* is used to measure the pressure difference between two pressure points. It is connected to a carrier demodulator which powers the sensor and converts the signal to an analogue signal. The manual [25] provides detailed information on the working principle, calibration, and usage, which will be discussed below.

Variable reluctance principle

Inside the DP15 there are two cavities separated by a membrane. In our case the cavities are filled with water. One cavity is attached to the upstream pressure hole and the other to the downstream one. A pressure difference between the two cavities is thus present and this is the quantity of interest.

At each side in the body, a coil is located through which an oscillating current is flowing generating a magnetic field. The magnetic field of one coil influences the other (Lenz' law). The resistance to a magnetic field is called the magnetic reluctance. The membrane is made of a magnetic permeable material (stainless steel) and influences the magnetic reluctance of the coils. For zero pressure difference the membrane is not deflected and the magnetic reluctance for both coils is equal. Due to a pressure difference the membrane deflects towards the lower pressure side and the magnetic reluctance of one coil increases whereas the other decreases. The carrier demodulator detects the change due to the deflection and provides a measurable volt signal which depends linearly on the pressure difference.

Figure 4.5 displays the transducer bridge circuit on the left and a picture of the internal structure of the sensor on right. This picture is taken after cleaning with ethanol.

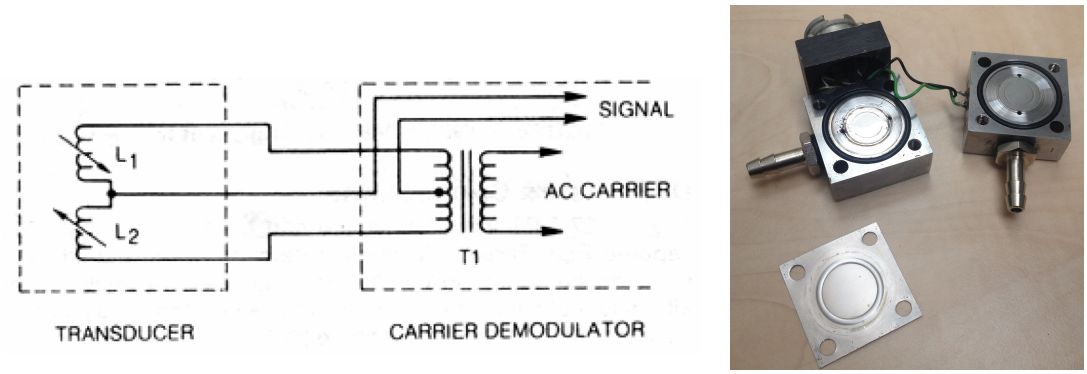

Figure 4.5: Valydine electronic pressure transducer. *Left*: Transducer bridge circuit [25]. *Right*: Internal structure of the differential pressure transducer DP15 after cleaning. A diaphragm, at the bottom, separates the two internal cavities.

The *Validyne* DP15 pressure transducer has an interchangeable membrane, making it a very versatile device. By selecting the correct membrane, the maximum pressure difference can be chosen from 0.88 kPa up to 35 MPa. The membrane can withstand up to two times its maximum pressure, but does not provide a linear signal in overpressure.

Previous measurements on core-annular flow performed by Ingen Housz [24] suggest a maximum pressure difference of approximately 2000 Pa. To be on the safe side, a diaphragm with a maximum of 3500 Pa is chosen.

Before calibration, the pressure transducer and carrier demodulator are tested for functionality using tutorial videos published by *Validyne Engineering* [26, 27].

4.5.2 Calibration

The differential pressure transducer is calibrated by using two static water columns attached to either side of the DP15, see figure 4.6. The column connected to the lower pressure side is kept at a constant level, whereas the water column attached to the higher pressure side is varied to generate a pressure difference between the two sides. The pressure difference, ΔP, due the height difference, Δh, is calculated as:

$$\Delta P = \rho_w \, g \, \Delta h \tag{4.1}$$

The settings on the carrier demodulator are now adjusted to show 0.0 pressure difference at 0.0 V and the maximum calibration pressure of 2500 Pa at 9.5 V. This is an iterative procedure where the *zero* adjustment must be the final change. After the final setting, the final calibration curve is made and given in figure 4.7. As expected a linear relation between the output signal and the pressure is obtained. The linear fit has an R^2-value of 0.9996 which indicates an almost perfect fit.

However, it should be noted that the output signal at zero pressure difference drifted from day to day. Even when the carrier demodulator is heated up (approx 30 minutes), this effect

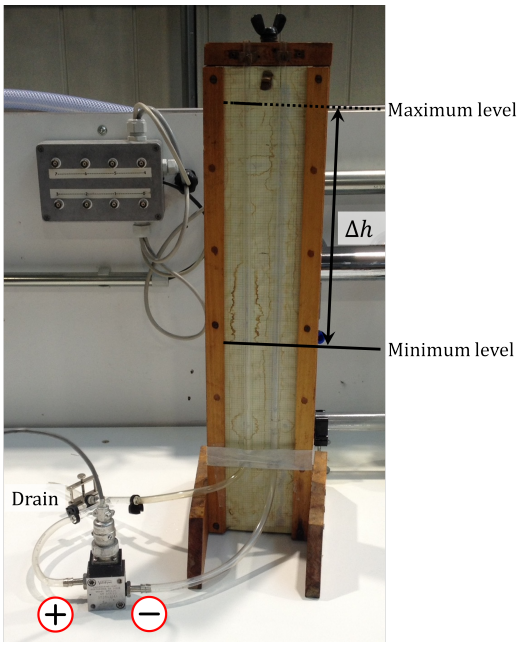

Figure 4.6: Configuration for the calibration of the differential pressure transducer by means of static water columns. On the left side the drain and the high/low pressure sides of the transducer are indicated. On the right the minimum and maximum water levels are displayed.

remains present. The shift is in the order of 0.1 to 0.2 V which corresponds to 1 to 2 percent of the maximum span. The behaviour of the maximum set pressure was also checked due to this observation. It is concluded that only the zero point is shifting and the slope of the calibration curve remains unaltered.

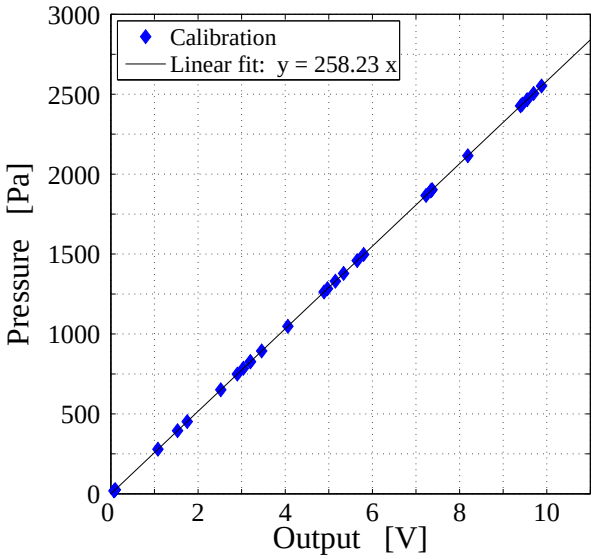

Figure 4.7: Calibration points to relate the output signal of the pressure transducer to the pressure. The linear curve fit is also included.

To correct for this error, before every measurement series a zero measurement is performed to determine the zero of that day, p_{zero} in volt. The used calibration curve is now given as:

$$[\text{Pa}] = 258.14 \cdot (Volt - p_{zero}) \tag{4.2}$$

4.5.3 Check of the calibration

After all experiments, the pressure sensor is checked for its calibration. The result is presented in figure 4.8. The zero correction described above is applied for the calibration check. At first sight, it seems that both curves follow the same line. However, the slope of the linear fit of the calibration check is smaller. Using both linear relations at 10 V, the maximum pressures are 2581.4 Pa and 2471.9 Pa for the original and checked calibration curves, respectively. This is a difference of 4.4 percent.

It is hard to explain the difference since it depends on many parameters, such as the configuration of the calibration set-up, the water density, electronic stability of the power supply or contamination inside the sensor cavities. A statement on which calibration curve is the correct one is even harder to make. It certainly is a factor of error in the pressure drop measurements.

For the data analysis part of the project, the first calibration relation with adjusted zero pressure difference, equation (4.2), is used to convert the output signal to a pressure.

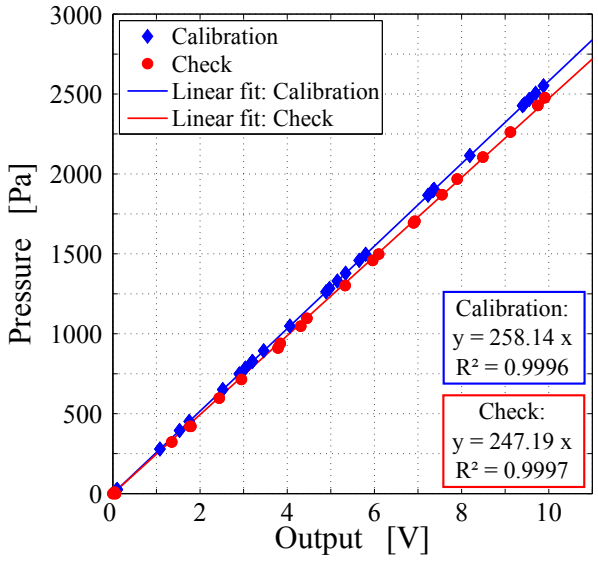

Figure 4.8: Calibration check of the differential pressure transducer.

4.6 Visualisation section

The purpose for the new visualisation section is to analyse and characterize the shape of the oil-water interface in core-annular flow from multiple directions. The top and bottom of the interface can be captured by a camera horizontally aligned with the pipe. This image is called the front view. Looking from above, the front and back of the core in the horizontal plane can be captured in a top view.

One way to acquire images from multiple directions is to use multiple cameras. In this case a triggering system is required to link the multiple images together in time. Another option is to use a mirror to display the front and top view in a single image. The two views are now automatically synchronised. This configuration has the advantage of using only one high-speed camera and no triggering system is required. The approach with the mirror is chosen and is further described in this section.

The curvature of the pipe causes undesired refraction of light, especially in the regions of interest, e.g. the top and bottom of the core in the front view. By replacing the medium around the pipe with a medium with a higher refraction index the refraction from the pipe wall is reduced and the images show less distortion. A medium with the same refraction index as the pipe would be ideal. Just water proved to be sufficient. For this purpose a symmetric box is built around the pipe.

The table of the set-up limits the available space under the pipe. Therefore the mirror is place on the top of the imaging box. This requires the imaging box to be closed off by an additional plexiglass plate. External vibrations, e.g. from the oil pump, can create distortions on the free surface and the top view gets corrupted. Two tubes are located on each side such that the container can be filled and drained.

The used mirror is a first surface mirror of high quality and is placed under an angle of 45° on top of the imaging box. Figure 4.9 displays the end result of the new visualisation box with mirror. The length of the imaging section is approximately five times the inner pipe diameter.

4.6.1 Optical path length correction

The optical paths for the front and top view differ since the top view is observed via a mirror. There are two solutions to have both views in focus.

The first possibility is changing the aperture of the camera: a smaller aperture results in a larger focal depth. However, reducing the aperture size also decreases the amount of light on the optical chip. Since the exposure time will be very short this is an undesired effect.

An other possibility is to place a medium in between the longer path length such that it is perceived at a closer distance. For example, an object in a swimming pools appears closer

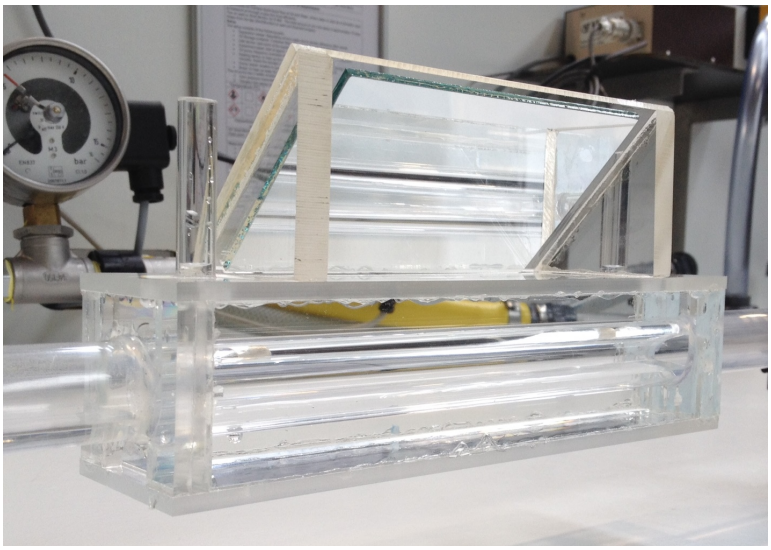

Figure 4.9: Photograph of the realized visualisation section.

than it is actually located. The thickness of this medium depends on its refractive index. A small aquarium made of PMMA with 3 mm thick walls has been used to correct the path length. The thickness of the water layer now needs to be calculated.

The imaging box around the pipe is symmetric for both views. The difference in path length between the front and top view, ΔL, is determined by:

1. the vertical path length from the top of the imaging box to the mirror and
2. the horizontal path length from the mirror to the plane determined by the front of the imaging box.

This length is measured to be 38 mm. The refractive indices for air, water and PMMA are $n_{air} = 1.00$, $n_{water} = 1.33$ and $n_{pmma} = 1.49$ respectively. The thickness of the water layer, x, is calculated as:

$$\Delta L = [2d_{pmma}\, n_{pmma} + x\, n_{water}] - (2d_{pmma} + x)n_{air} \tag{4.3}$$

$$x = \frac{\Delta L - (n_{pmma} - n_{air})2d_{pmma}}{n_{water} - n_{air}} \tag{4.4}$$

The wall thickness, d_{pmma}, is 3 mm. The thickness of the water layer is calculated to be 106.2 mm to correct for 38 mm of extra path length. Note that the correction box replaces a certain path length through air. This is the last term on the right side of equation (4.3).

4.7 Replacing the oil

The set-up is in operation since 2015 and the oil properties have changed. The used oil is *Morlina S4 B 680*. Over time the oil has absorbed some water and the viscosity has decreased with approximately 20% at 20°C [28]. Since water is absorbed it is also possible that the interfacial tension has changed over time. Therefore it was decided to replace the oil.

First all oil is removed from the separation barrel. In this vessel, a water layer is present at the bottom which thus is not in contact with air due to the oil layer on top of it. Bacteria have formed and died in this layer generating a nasty smell. Using water, a brush and cleaning paper the separation vessel is fully cleaned. No detergent is used since it can remain in the vessel and then influence the oil properties. The result is given in figure 4.10.

After cleaning, first a layer of water is poured in followed by oil. After a day, the fluids are separated. The old oil remaining in the small pump and in the attaching hoses was replaced by pumping some oil and collecting it in a bucket. The new oil has a different colour, so it can be seen when all old oil has been removed.

Figure 4.10: Photographs of the inside of the separation vessel. Left: Vessel after all fluids have been removed. The black residue are dead bacteria mixed with oil. Right: Clean inside of the separation vessel.

The oil container has also been fully emptied and cleaned with paper. A small layer of water was found at the bottom of the container. The oil storage container is then filled with new oil.

The last part is to replace the oil in the main oil pump and connected hoses. This is done in a similar way as for the small oil pump and connected hoses. Now all old oil is replaced by new oil.

Chapter 5

Experimental Procedure

Based on the fluid properties, described in chapter 3, and on the details of the experimental set-up, described in chapter 4, the conditions for the experimental campaign are defined. This will be discussed in the first part. The procedure taken to perform an experiment is described afterwards. This chapter is concluded with the results of a typical experiment.

5.1 Experimental conditions

The selection of the final set of experimental conditions has been the result of an iterative process, in which the results were analysed intermediately to determine the following set of experiments. The choices made in this process are discussed here.

The first experiments were preformed to obtain experience with the set-up and with the new pressure sensor in particular. The aim of these experiments was to determine the reproducibility of the results and to compare them with previous results described in the master thesis of Ingen Housz [24]. An intermediate oil flow rate of 0.35 l/s was chosen at which the watercut was varied.

First, two experiments were performed per batch of oil as was also done by Ingen Housz. This means that two experiments could be performed per day. In the pressure signal, see section 5.3.1, a settling time is observed and fluctuations in the signal. To obtain a more reliable pressure signal, it was decided that longer experiments are favourable. The choice is made to perform one 'long' experiment per day of approximate 1.5 minutes. Since time of the project is limited, choices have to made on further experiments.

After the first experiments to test the reproducibility and compare the data with previous work, the oil viscosity will be changed by heating it up. This is where the iterative approach is most clear. For example, oil temperature intervals were set at 10 °C from 20 °C to 50 °C.

Since the oil viscosity varies more at lower temperature, a gap in the realized viscosity range was noted. Extra experiments at 25 °C were performed to obtain a more evenly distributed viscosity range.

The final set of experimental conditions to investigate the influence of the viscosity is given in table 5.1. The oil kinematic viscosity corresponding to the oil temperature is given for reference. It must be noted that at room temperature, more values of the watercut were investigated in order to compare the results with Ingen Housz. The watercut was varied between 9% and 15% with 1% percent intervals and at 20% and 25%.

Table 5.1: Final set of experimental conditions to determine the influence of the oil viscosity on core-annular flow.

Parameter	Value / Range	
Oil flow rate	0.35	l/s
Watercut	9, 12, 15, 20, 25	%
Oil temperature	20, 25, 30, 40, 50	°C
Oil kinematic viscosity	3340, 2190, 1470, 720, 380	cSt

5.2 Experimental procedure

The procedure of performing an experiment is given below. An extended version of the operation protocol for the core-annular flow set-up is attached in Appendix C. As explained in the next chapter, only one experiment is done per day, i.e. all oil available in the oil storage container is used for a single experiment.

The experimental procedure is as follows. The items indicated with a $\star$ are required for visualisation.

- Turn on DP15 power supply and computer(s). Run LabVIEW and check for errors.
- Pump over oil from separation barrel and dispose waste water afterwards.
- Calculate the setting for the experimental conditions.
- *Optional*: Heating up the oil:
  - Set oil valve to circulation and turn on heating system.
  - Start oil pump and run at maximum flow rate.
  - Disable heating system and just before when the desired oil temperature is reached. Let the oil pump run longer for uniform temperature.
- Connect all pipes in flow loop. Run water flow only to fill the pipe and connect the pressure transducer.

- Stop water flow and oil pump. Perform a zero pressure difference measurement.
- *Optional*: At room temperature: Let the oil circulate for 1 minute.
- Pre-set oil flow rate.
- ⋆ Check the visualisation section, correction box and lights for image acquisition.
- Start LabVIEW data acquisition (Stop, name file, start).
- Set the desired water flow rate.
- Open experiment oil valve and start oil.
- ⋆ Capture images when the flow is fully settled.
- Stop oil pump and close experiment valve.
- Clean the flow loop using the rinsing system, flush with warm water only afterwards.
- Disconnect all pipes.
- Save LabVIEW data appropriately.
- ⋆ Save recorded images.
- Close main water supply, turn off all electrical devices.

5.3 Typical experiment

A short MATLAB routine is written to easily analyse an experiment and to extract averaged signals of the experiment for further processing. The recorded data of a typical experiment as function of time is discussed below.

In this case, the predefined setting are an oil flow rate of 0.35 l/s, 15% watercut and room temperature. To recall, the sampling rate of the differential pressure, temperature and oil flow rate sensor is 100 Hz and the water flow rate is sampled at 1 Hz.

5.3.1 Pressure signal

The signal of the pressure drop is given in figure 5.1 and clearly shows the different stages of an experiment. The boundaries of the different stages are included as vertical dashed red lines in the figure. For These boundary indicators are included in the figures for the oil flow rate, water flow rate and oil temperature as well.

In part 1, the water flow rate is set to maximum and afterwards decreased to the desired setting. This can be seen in the decrease in differential pressure around 50 s. The oil pump is

turned on and is the start of part 2. Activating the oil pump causes a spike in the signal due to a power surge. Afterwards the pressure drop starts to increase with increasing oil flow rate. The maximum pressure value is reached slightly later after reaching the pre-set oil flow rate. Now the flow needs to settle to determine the pressure drop in stable flow conditions. This is observed in the slight decrease in the signal. The residence time of the fluids is approximately 8 s based on the mixture velocity and total length of the flow loop from divider to separation barrel. The stabilization time is almost twice this time.

Stable core-annular flow is achieved in part 3. The mean value of the signal is indicated with the solid red line. Fluctuations around the mean are observed and are in the order of ±200 Pa/m for all experiments. The oil pump causes electric noise in the electrical system, as will be discussed in section 5.3.2. This contributes to a part of the fluctuations. It is hard to put a number on this disturbance, because the water flow rate is limited to reproduce the obtained order of the pressure drop.

Due to the wave structure on the interface, the composition of fluids above one pressure point varies and thus also the density of this fluid column. However these fluctuations are in the order of 3 Pa and have therefore a negligible effect on the pressure signal.

More important are the velocity variations in the annulus due to the wavy interface. The levitation mechanism, see section 2.3, is based on the variation of the velocity, generating higher and lower pressure regions around the core. This creates a net downwards hydrodynamic force to counterbalance the buoyancy force.

The Reynolds number based on the superficial velocity of the annulus and its fluid properties is determined at 3200, which means that the flow in the annulus is turbulent. This was also confirmed in [29] by dye injection into the annulus. The variations in velocity, due to

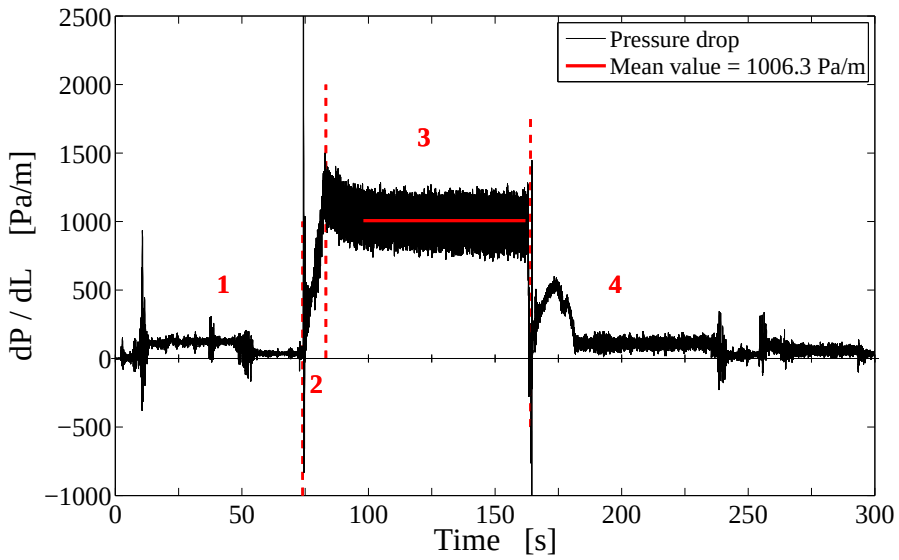

Figure 5.1: Pressure drop signal as function of time for a typical experiment.

turbulence and the waves on the oil-water interface, are causing the pressure fluctuations observed during stable core-annular flow.

After the experiment, the oil pump is turned off causing a negative peak in the signal due to a power surge. This is seen in part 4. The water flow rate is set to maximum. Around $t = 250$ s the water flow rate is decreased and later increased again to minimize oil drops remaining in the flow loop.

5.3.2 Oil flow rate

The volumetric oil flow rate as function of time for the typical experiment is given in figure 5.2. The oil pump is turned on at $t \approx 75$ seconds and reaches the pre-set oil flow rate at $t \approx 83$ s. At the end of the experiment, the oil flow rate is decreased in approximately 2 seconds and turned of at $t \approx 164$ s. A gentle reduction of the oil flow rate is favourable to reduce fouling due to instabilities at the end of an experiment.

An oscillation of $\frac{1}{13}$ Hz is observed in the signal during operation of the oil pump. However, this oscillation is also present when the pump is turned off. Hence, it can be concluded that this is not a physical variation in the oil flow rate. Since longer experiments are performed, the influence of the oscillation is not influencing the averaged value indicated with the red line. The oscillation is very likely caused by the frequency modulator which controls the oil pump. Even when the pump is turned off, the modulator is active and the slow oscillation is present in the signal.

When the oil pump is running, electrical noise is present in the signal. This is observed in

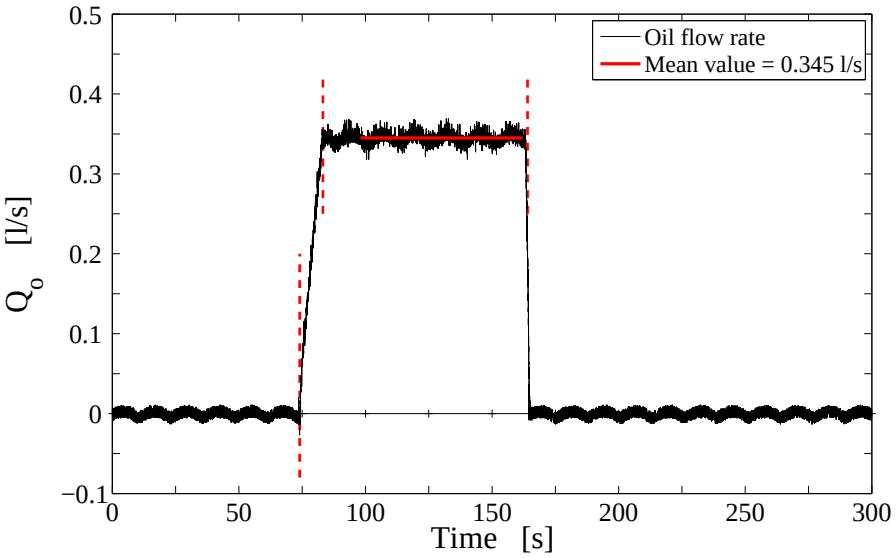

Figure 5.2: Volumetric oil flow rate as function of time for a typical experiment.

high frequency oscillations with larger amplitude when the pump is turned on. For zero oil flow rate, these disturbances are not present in the signal.

5.3.3 Water flow rate

The water flow rate is presented in figure 5.3 and it can clearly be seen that this signal is digital. At start, the water flow rate is set to maximum and afterwards adjusted to the desired water flow rate for the experiment. After an experiment the water flow rate is set to maximum to reduce fouling. The flow rate is changed around $t \approx 250$ s, which confirms the fluctuations in the pressure signal. At this time, an oil drop detached from the inlet device when the water flow rate was decreased. In reaction, the water flow rate is increased again to flow this drop trough the flow loop to avoid fouling.

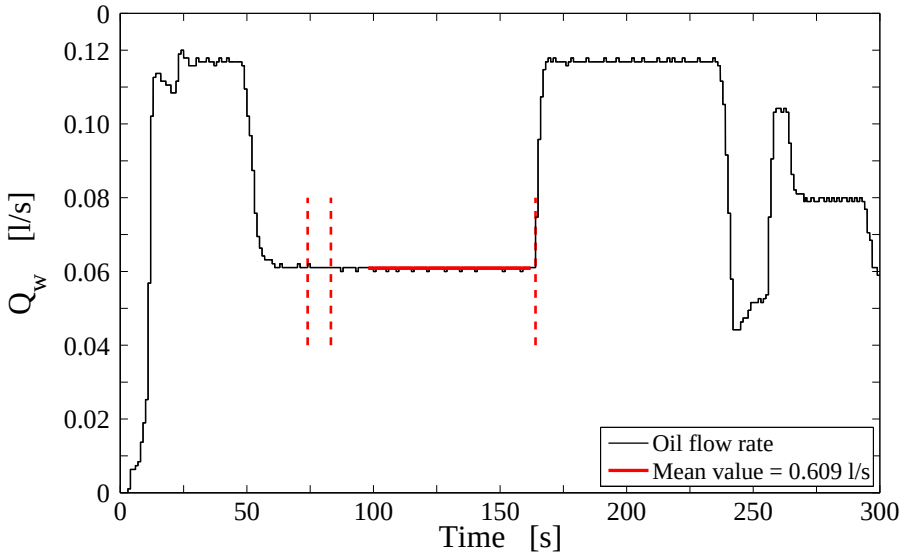

Figure 5.3: Volumetric water flow rate as function of time for a typical experiment.

5.3.4 Temperature signal

The analogue temperature signal is presented in figure 5.4. The red line is the averaged value during the core-annular flow experiment.

It is immediately observed that the signal contains much fluctuations, before the oil flow is started. The sensor is place just prior to the divider where oil is still present in the supply line. All components are in contact with ambient conditions and must therefore be at ambient temperature. Hence, fluctuation of $\pm 1°$C is not physical. Details of the sensor itself are not available which makes it difficult to find the nature of the noise. The averaged signal is observed to be a representative value of the actual oil temperature.

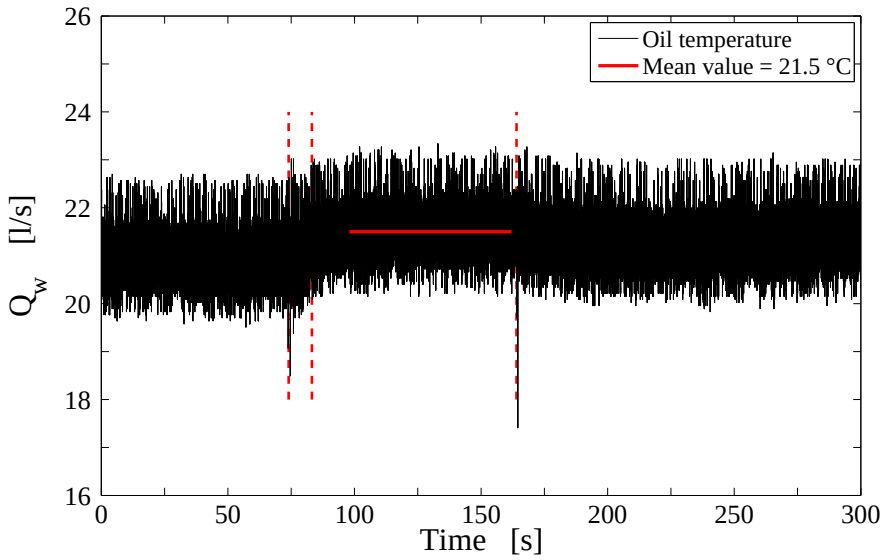

Figure 5.4: Oil temperature as function of time for a typical experiment.

5.3.5 Data extraction

The start and end time of the stable core-annular flow are determined from all graphs presented above. The duration of an experiment is typically around 60 s. The averaged values of the signals are computed within these time constraints and are included as the solid red line in the graphs above.

The averaged signals are stored in a separate file for later processing. A combined graph of all signals is saved for later reference.

Chapter 6

Pressure Drop Results

In this chapter the results of the pressure drop measurements for core-annular flow will be presented. Before the main results are presented, the scaled pressure drop is introduced. Thereafter, the experiments performed at room temperature will be presented and compared to previous results by Ingen Housz et al. The influence of the oil viscosity on the measured pressure drop will be discussed in detail. To conclude the pressure drop results, two models to predict the pressure drop are tested.

6.1 Scaling of the measured pressure drop

The measured pressure drop for core-annular flow will be scaled by the pressure drop of single phase oil flowing at the same conditions as in the two-phase experiments, i.e. the same oil flow rate and the same oil viscosity. This scaling can be interpreted as a reduction factor when comparing the pressure drop for core-annular flow and single phase oil flow.

First, the Reynolds number for single phase oil flow is determined, which is based on the superficial oil velocity and on the pipe diameter. The highest Reynolds number is at the lowest oil viscosity, resulting in $Re_{s,o} \approx 50$. The single phase oil flow is thus laminar and its corresponding pressure drop over a pipe length dL is calculated as:

$$\left(\frac{dP}{dL}\right)_{oil} = \frac{128}{\pi} \frac{\mu_o Q_o}{D^4} \tag{6.1}$$

The scaled pressure drop is defined as:

$$\frac{(dP/dL)_{CAF}}{(dP/dL)_{oil}} = \frac{dP_{CAF}}{dP_{oil}} \tag{6.2}$$

6.2 Comparing results

The results at room temperature are compared to previous results by Ingen Housz et al. [29, 24], who used almost the same set-up as in this study. They used an inverted U-tube manometer to measure the pressure drop, whereas an electronic pressure transducer is used here. As viscous liquid they used *Morlina S4 B 680* with an density of 860 kg/m^3 and a kinematic viscosity of 2910 cSt at room temperature. The viscous oil in the present study is *Morlina S2 B 680* with a density of 913 kg/m3 and viscosity of 3010 cSt at room temperature. Both experiments are performed at an oil flow rate of 0.35 l/s at which the watercut is varied. The results are shown in figure 6.1 where the scaled pressure drop is presented for various watercuts.

Overall a similar trend is observed between the two sets of experiments, where a minimum in the scaled pressure drop is found at a watercut between 10% and 14%. In general, the present measurements for the pressure drop are lower than those measured by Ingen Housz et al. A first explanation for the difference is the oil viscosity at room temperature. Comparison of the kinematic viscosity of the oil shows a slightly lower value as in the experiments by Ingen Housz et al. As will be discussed later, decreasing the oil viscosity will increase the scaled pressure drop, dP_{CAF}/dP_{oil}. Since the oil viscosity in the present experiments is slightly larger, the value of the scaled pressure drop is smaller.

A second reason for the difference in the scaled pressure drop is the density difference between oil and water. Since the oil density in the present experiments is higher, the density difference between oil and water is smaller. Therefore, the upward buoyancy force on the core is lower, which leads to a less eccentric oil core. The water annulus at the bottom becomes thicker

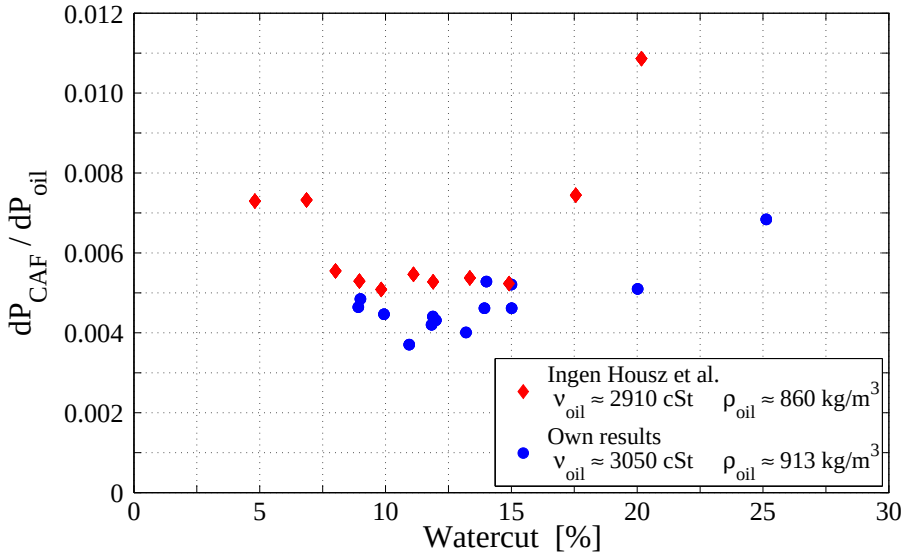

Figure 6.1: Comparison between the results by Ingen Housz et al. [29] and the present results for the scaled pressure drop as function of the watercut.

when the core is more eccentric. Since the pressure points are located at the bottom of the pipe, the pressure measurements could be influenced by the thicker water layer. Especially for a larger watercut ($> 18\%$) this effect becomes more dominant, which might contribute to the deviation between the two experimental data sets.

Furthermore, it is mentioned by Brauner [12] that friction at the oil-water interface contributes to the overall pressure drop and becomes more significant when the core is located more eccentrically. This also explains the overall lower pressure drop in the present results.

6.3 Pressure drop for varying oil viscosity

Figure 6.2 displays the results for the scaled pressure drop as function of the watercut. At room temperature, which gives $\nu_o \approx 3050$ cSt, the watercut is varied with smaller increments.

For the highest oil viscosity, the minimum is observed around 12% watercut. This minimum is not observed any more for decreasing oil viscosity. In general the scaled pressure drop decreases for decreasing watercut. In the limit case of 0% watercut, the measured pressure drop will be equal to pressure drop for oil only and thus equal unity. From the decreasing behaviour of the scaled pressure drop with decreasing watercut and the limit case of 0% water cut, a minimum is expected to form at lower watercut than presented here.

Further experiments can be performed to find the minimum in dP_{CAF}/dP_{oil} at lower oil viscosities. For industrial applications, however, such small watercuts might be infeasible due to the increased risk of fouling when using a thin lubrication layer.

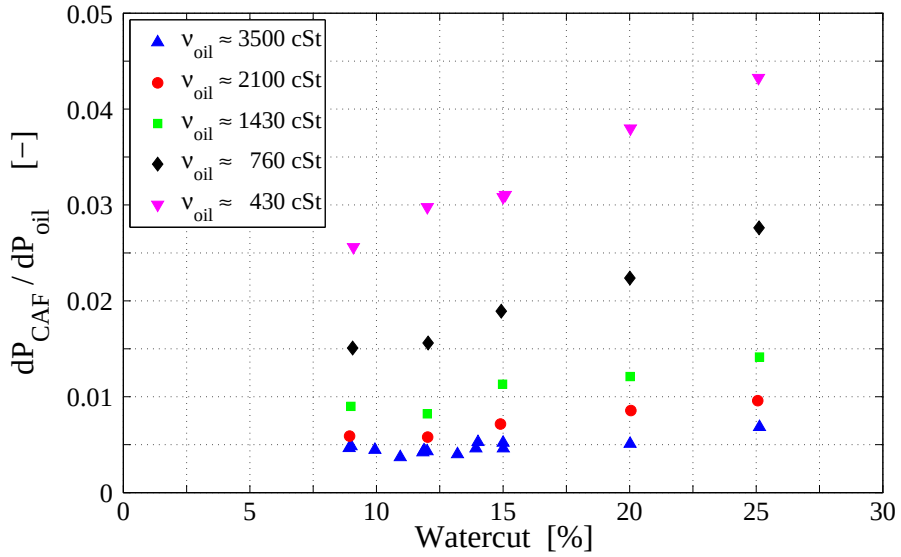

Figure 6.2: Scaled pressure drop as function of the watercut for different values of the oil kinematic viscosity.

Figure 6.3 presents all values of the measured (non-scaled) pressure gradient, dP_{CAF}/dL, as function of the oil kinematic viscosity, ν_{oil}, for different values of the watercut. The oil viscosity decreases with increasing temperature; the viscosity varies between about 3000 cSt at 20 °C and about 400 cSt at 50 °C.

At the considered watercuts, there seems to be a trend that the pressure gradient decreases with decreasing oil viscosity. At the largest considered watercut of 25% the pressure gradient is almost independent of the oil viscosity. For all oil viscosities, an increasing watercut gives an increase of the scaled pressure gradient. This is due to the increase in the water flow rate at constant oil flow rate, which results in a larger total flow rate.

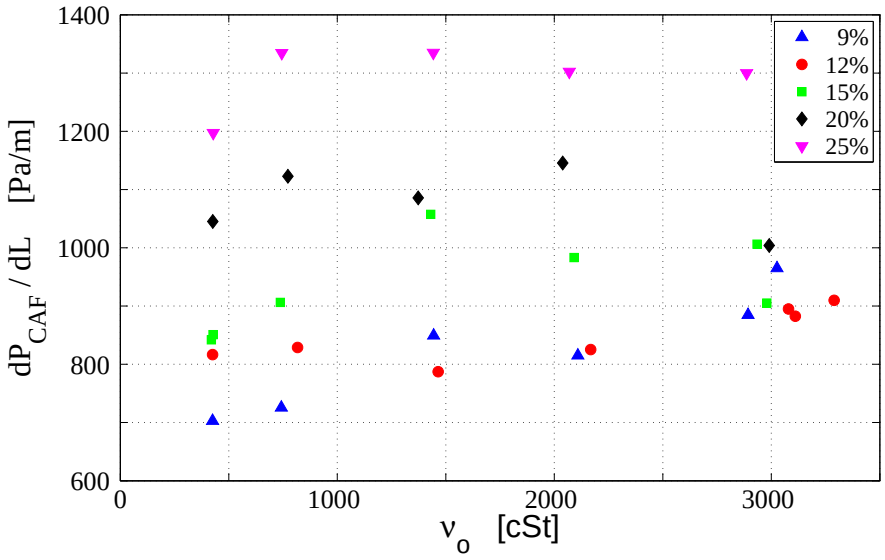

Figure 6.3: Measured pressure drop as function of the oil kinematic viscosity for different values of the watercut.

Figure 6.4 gives an overview of all values of the measured scaled pressure drop as a function of the viscosity ratio of the high and low viscous fluids, ν_o/ν_w, at all considered watercuts. With increasing temperature, the viscosity ratio decreases. It ranges between $\nu_o/\nu_w \approx 400$ at 50 °C and $\nu_o/\nu_w \approx 3000$ at 20 °C.

As described by equation (6.1), the pressure drop for single phase oil depends on the pipe diameter, oil flow rate and oil viscosity. Only the latter one is varied, from which it is expected that the scaled pressure drop increases with decreasing oil viscosity.

Figure 6.4 shows that dP_{CAF}/dP_{oil} decreases with increasing viscosity ratio. This means that the relative advantage of adding water to form a lubrication layer along the pipe wall is larger if the oil is more viscous. The figure also shows that for the highest considered oil viscosity, i.e. the one at room temperature, the value of the scaled pressure drop is almost independent of the watercut. But for a decreasing viscosity ratio, the scaled pressure drop increases with the watercut. The benefit of water lubrication at low oil viscosity is less. Even for the lowest viscosity ratio the pressure drop at core-annular flow is significantly lower than for single phase oil flow.

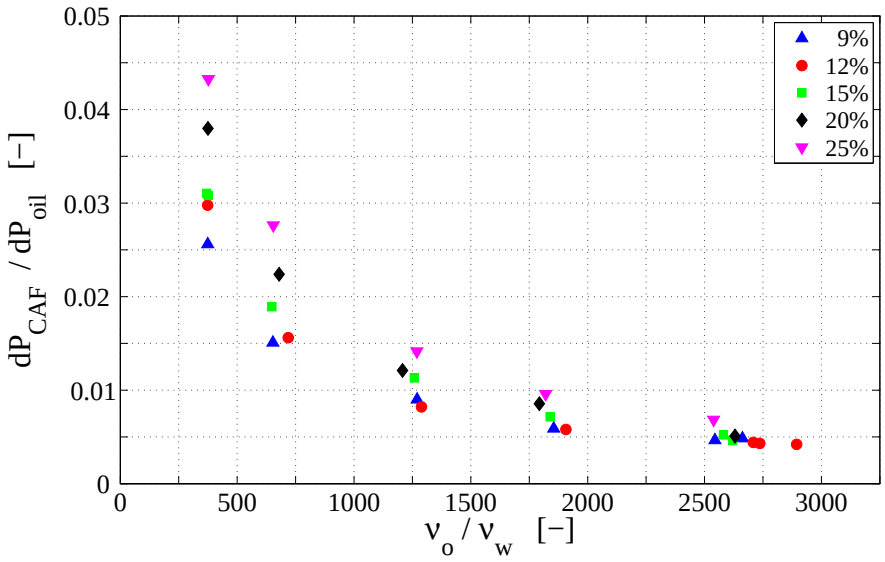

Figure 6.4: Scaled pressure drop as function of the viscosity ratio for different values of the watercut.

The experiments were performed at a fixed oil flow rate, which means that increasing the watercut results in a larger total flow rate. At low viscosity ratio, the increase of the total throughput reduces the benefit of using water for lubrication even more.

6.4 Other scaling factors

Several attempt have been made to scale the the pressure drop data onto a single curve. The Froude number based on the density difference did not result in such result, nor did it provide further insight in the influence of the viscosity.

6.4.1 Reynolds number based on pseudo fluid

When regarding the core-annular flow as a single pseudo fluid, as in the model of Bannwart [13], the Reynolds number can be expressed as:

$$Re_{pseudo} = \frac{\rho_{mix} u_{mix} D}{\mu_{mix}} \tag{6.3}$$

with the mixture density, ρ_{mix}, given in (2.7) and the mixture viscosity, μ_{mix} defined as:

$$\frac{1}{\mu_{mix}} = \frac{(1 - H_w)}{\mu_o} + \frac{H_w}{\mu_w} \tag{6.4}$$

The hold-up is determined by relation (2.4).

The scaled pressure drop as function of the Reynolds number based on the pseudo fluid is given in figure 6.5. The observed trends are almost identical to those in figure 6.2, where the scaled pressure drop is given as function of the watercut. Additional information on the behaviour is unfortunately not obtained.

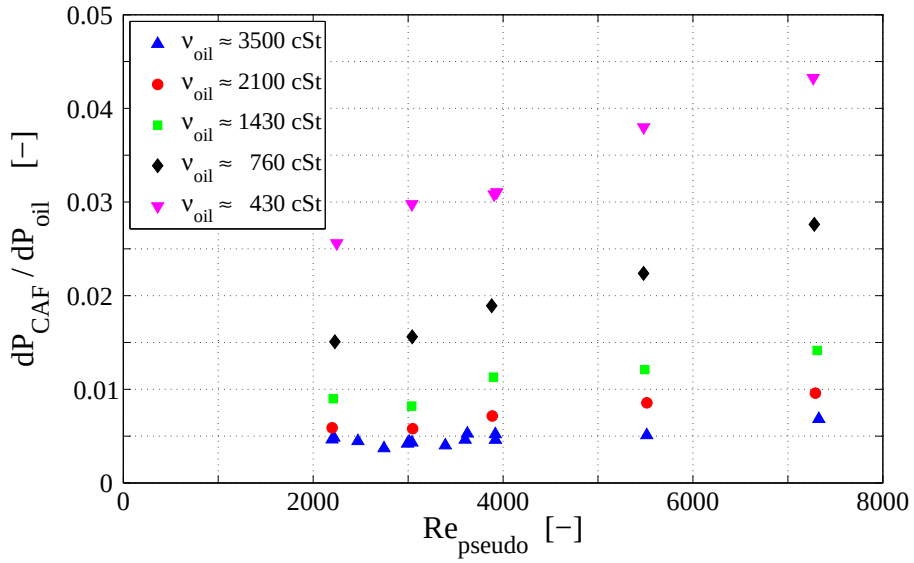

Figure 6.5: Scaled pressure drop as function of the Reynolds number for a pseudo fluid, defined in equation (6.3). Different values for the oil viscosity are shown.

It must be noted that for a large viscosity ratio and for comparable densities of the oil and water, the mixture Reynolds number can be approximated by equation (6.5) below [13]. This explains the similarity between the result in figure 6.2 and figure 6.5. The only varying parameter in $Re_{s,w}$ is the superficial velocity, $u_{s,w}$, which is proportional to the water flow rate. Using equation (2.2a) to rewrite the water flow rate in terms of the watercut, the superficial water velocity is proportional to $C_w/(1 - C_w)$.

$$Re_{pseudo} = \frac{\rho_{mix} u_{mix} D}{\mu_{mix}} \cong \frac{\rho_w u_{s,w} D}{\mu_w} = Re_{s,w} \tag{6.5}$$

6.4.2 Reynolds mixture number

Based on the idea of a pseudo fluid, a different definition for the mixture viscosity is tried. Since the mixture density is the weighted average of the separate densities of oil and water, the mixture viscosity is calculated in similar way as:

$$\mu_{mix} = (1 - H_w)\mu_o + H_w \mu_w \tag{6.6}$$

The Reynolds number is determined as stated in equation (6.3), but now with the modified mixture viscosity.

Figure 6.6 displays the scaled pressure drop as function of the mixture Reynolds number, based on the modified mixture viscosity. All data point collapse onto a single curve, which seems to be the desired result.

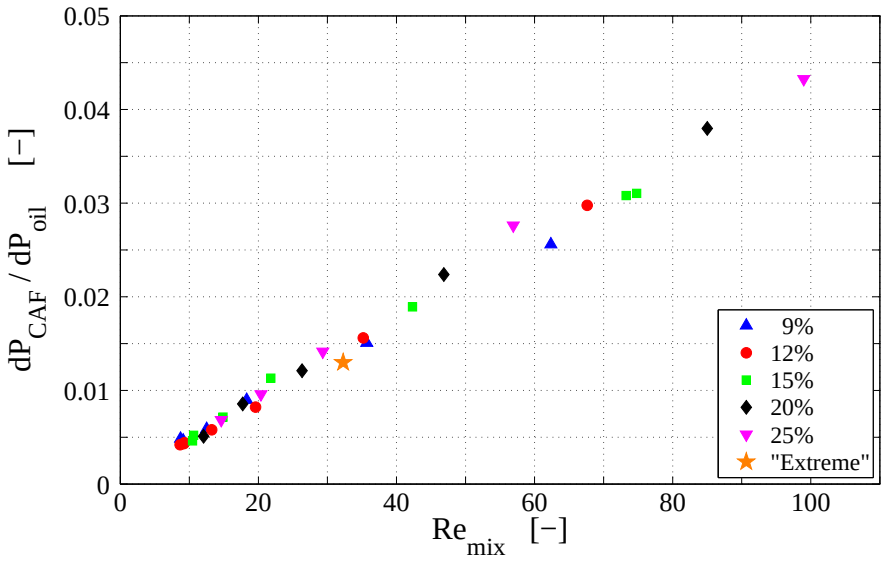

Figure 6.6: Scaled pressure drop as function of the mixture Reynolds number, where the modified mixture viscosity is defined in equation (6.6).

However, the physical nature of the modified mixture viscosity is not very clear. While the mixture viscosity based on a pseudo fluid is derived from the governing flow equations [13], the weighted averaged mixture viscosity is simply stated.

Computational fluid dynamics for two phase flow, using a volume of fluid approach, uses fluid property averaged values to determine the fluid parameters in a cell. Based on the volume fraction per cell the effective viscosity of that cell is calculated as the weighted average. This is done on a micro level, where an interface can span over multiple cells. Using the same approach to a full scale situation, as with core annular flow, is questionable from a physical perspective.

Many viscosity models in the literature deal with emulsions of one phase into a continuous phase. An example is Einstein's equation for the effective viscosity of low dispersed phase volume fractions [30]. In core-annular flow, both phases are separated distinctly and, therefore, viscosity models based on dispersions are not applicable.

Additional experiment

The experiments were performed for one fixed value for the oil flow rate (0.35 l/s). It could be possible that the proposed scaling with Re_{mix} is the result of this limitation. To test this hypothesis, an additional experiment is performed at more extreme conditions. The oil flow rate is set to 0.5 l/s and a watercut of 15%. The oil viscosity is set at 1430 cSt ($\sim$ 30 °C), which results in a Reynolds mixture number of $Re_{mix} \approx 32$. This data point is included in

figure 6.6, labelled as '*extreme*'. It is seen that the additional data point has a similar scaling behaviour as the other measurements, i.e. it is located on the same trend line.

Although one additional experiment does not prove the hypothesis of a possible scaling factor, it can be a foundation for further research. For example, the pipe diameter is fixed for all experiments and Re_{mix} depends linearly on this parameter. In what extent the pressure drop of core-annular flow is influenced by the pipe diameter can be tested with results from known literature. This has not been done yet. The scaling results as presented here must thus be interpreted with care.

Conclusion on Reynolds mixture number

It is concluded that using a weighted average for the mixture viscosity in the scaling of the pressure drop for core-annular flow lacks physical foundation. However, using it for our pressure drop results give a very good linear dependence of the scaled pressure drop against the mixture Reynolds number. It is recommended to further analyse this. The influence of the pipe diameter has not been taken into account yet and further research is required here.

6.5 Comparison to theoretical models

The models by Brauner [12] and Bannwart [13], described in section 2.4, are tested against the obtained experimental data. The agreement between measurements and theory is presented in figures 6.7 and 6.8, where the solid diagonal line represent the perfect agreement. The dashed lines correspond to an accuracy interval of ± 20 %.

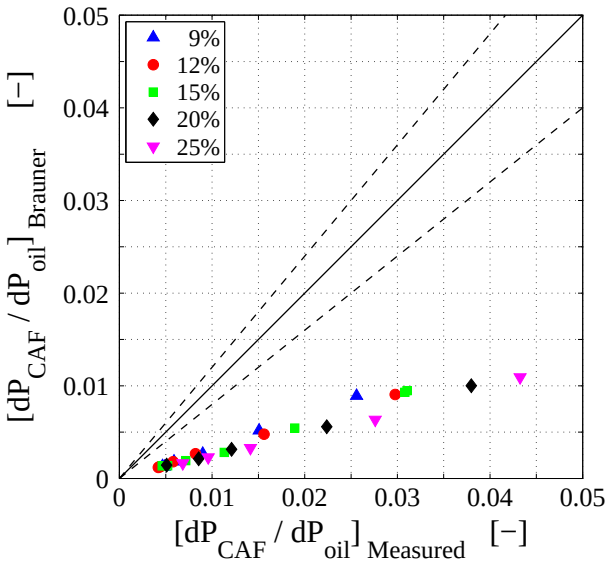

Figure 6.7: Comparison of the scaled pressure drop between the experiments and the two-fluid model of Brauner.

In the model by Brauner, see figure 6.7, the slip factor at the oil water interface, c_i, is set to 1.17 and the oil-water interface friction factor, F_i is set to one. Overall the model under predicts the measured values, which was already mentioned by Brauner. The measurements follow a linear increasing trend. This indicates that the model predicts similar behaviour, but is off by a factor of approximately 3.5. Different values for c_i have been tried though, without leading to a better agreement. Also various values for F_i are set, but without satisfying results.

A closer look at the intermediate steps did provide a possible explanation. The water hold-up according to Brauner, $\left(1-\tilde{D}_c^2\right)$, is significantly larger than the water hold-up determined by the emperical correlation of Arney et al. [7] (equation (2.4)). Averaged values of these values for different watercuts are given in table 6.1. The deviating factor is given in the last column. The analytically derived water hold-up by Brauner cannot be replaced directly with the emprical hold-up correlation of Arney et al. due to modelling assumptions. A more detailed study of the derivation is required.

Table 6.1: The water hold-up according to the model of Brauner [12] (column 2) and the empirical correlation for the hold-up according to Arney et al. [7] (column 3) for the different values of the watercut.

Watercut	$\left(1-\tilde{D}_c^2\right)$	H_w	$\frac{\left(1-\tilde{D}_c^2\right)}{H_w}$
9%	0.194	0.119	1.63
12%	0.256	0.157	1.63
15%	0.320	0.194	1.65
20%	0.424	0.256	1.66
25%	0.526	0.317	1.66

Figure 6.8 shows comparison between experiments and the pseudo-fluid model of Bannwart [13]. The Blasius set of $b = 0.316$ and $n = 0.25$ is used to evaluate the absolute pressure drop.

In general, the model over predicts the pressure drop. For the largest considered watercut, the agreement between the experiments and the model is better. Based on the Reynolds number of the annulus and the relative pipe roughness, different sets of b and n are used to evaluate the model [13]. In all cases, the model tends to over predict the absolute pressure drop.

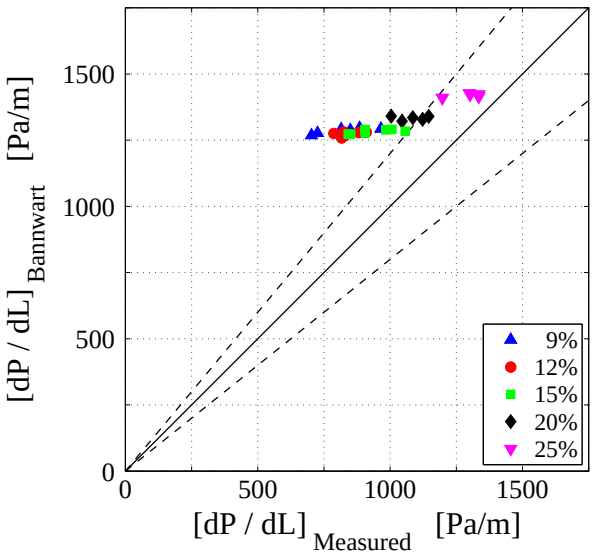

Figure 6.8: Comparison of the absolute pressure drop between the experiments and the psuedo-fluid model of Bannwart.

Chapter 7

Visualisation Results

Visualisation of core-annular flow is performed for varying oil viscosity and watercuts of 12% and 20 %. The results are given in this chapter.

7.1 Optical equipment

Flow visualization was realized using a *Vision Research* high-speed camera, with a 5 mega-pixel, 12-bit grey scale CMOS optical chip. The frame rate was set to 1000 fps and the exposure time to 80 μs. A *Nikon* lens, type Micro-Nikkor 105mm f/2.8D, is used, where the diaphragm is set at 5.6. A LED light panel is placed underneath the imaging box and an additional light source is placed near the imaging region to obtain sufficiently illuminated images.

Per experiment, 1000 frames are captured corresponding to 1 second of flow. The length of the recorded flow, based on the mixture velocity, is 1.14 m and 1.25 m for 12% and 25% watercut, respectively.

7.2 Images

Figure 7.1 to 7.4, at the end of this chapter, display typical flow patterns of core-annular flow at 20% watercut for four different oil viscosities. Figures 7.5 to 7.8 display core-annular flow at 12% watercut for the same range of oil viscosities. The flow is from left to right. The front view displays the flow as seen directly with the camera. The top view displays the flow as seen through the mirror, where the interface at the top is closest to the the camera. All images are post-processed to enhance the contrast of the oil water interface. The streamwise length of the images is approximately five inner pipe diameters. The bright spots on the core are reflections of the additional light source.

7.3 Discussion

Comparing the top and front view shows clearly the eccentricity of the core in the front view due to the upward buoyancy force. The top view displays the concentric core in the pipe. As expected, the water annulus becomes thinner when the watercut is decreased, making it harder to observe the interface at the top of the pipe. At some locations it seems that the oil core touches the pipe wall. Since no fouling is observed during the experiments, it can be concluded that the core is properly lubricated.

In all images waves are present on the oil-water interface. The front view shows that the wave crest, i.e. the interface closest to the wall, has a phase delay: the wave crest at the bottom is ahead of the wave crest present at the top of the core. In the top view, however, the wave crests are at almost the same streamwise location. This behaviour is more clearly observed for large watercuts (figure 7.1), but is also present at low watercuts.

The shape of the interface compared to the two levitation mechanisms (see figure 2.2) shows similarity to the 'flying core' model of Joseph et al. [10]. Looking at the front views, an isolated wave start with a steepening region which minimizes the thickness of the annulus. It is followed by a smoother region where the annulus becomes thicker. This wave pattern is observed in all recordings.

Decreasing the oil viscosity results in oil drops around the core. See for example the light grey circular objects in the middle of the core in the front view of figure 7.3. It is observed that these drops are formed at the divider where the oil core is injected. The oil drops are in the water annulus, but are still fully surrounded by water since the pipe wall is not fouled after a drop has passed.

When comparing the images for high and low oil viscosity, it is observed that the core is less smooth for low oil viscosity. The wave lengths present on the interface become shorter when the oil viscosity is decreased. Furthermore, a clear wave length is not observed any more. With decreasing oil viscosity, the oil can flow more easily and is thus more susceptible to deformations by hydrodynamic forces generated by the water annulus keeping the core lubricated.

For the lowest oil viscosity, see figure 7.8 for example, a large amount of oil drops are present in the annulus. The interface at the bottom in the frontview shows longer wave lengths on the interface compared to front view of 7.7. The oils drops prevent the core from forming smaller wave lengths.

7.4 Conclusion and further prospects

The flow visualisation study shows a clear distinction in the oil-water interface when decreasing the oil viscosity. The waves present on the interface become shorter in length and more irregular when the oil viscosity is decreased. This is observed for both large and small watercuts.

The images can be used to track the oil-water interface to obtain quantitative information of the flow. The core eccentricity, wave length and amplitude can be determined. The hold-up can be estimated and be tested to the hold-up correlation proposed by Arney et al., see equation (2.4). The derived information of core-annular flow can be used for comparison to numerical studies on the topic.

Top view

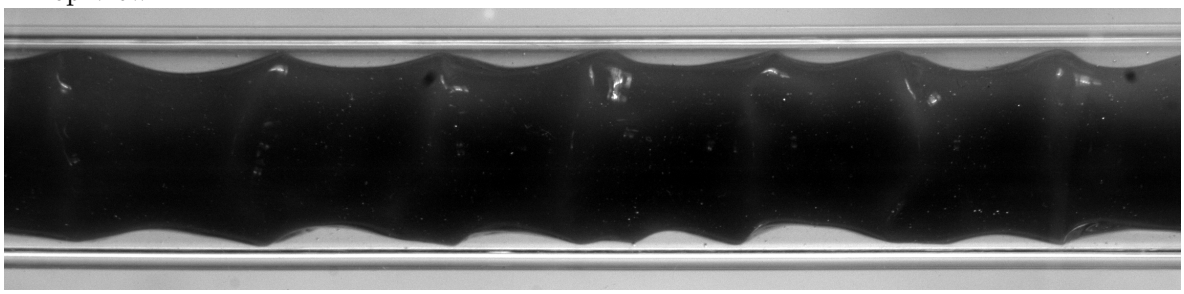

Front view

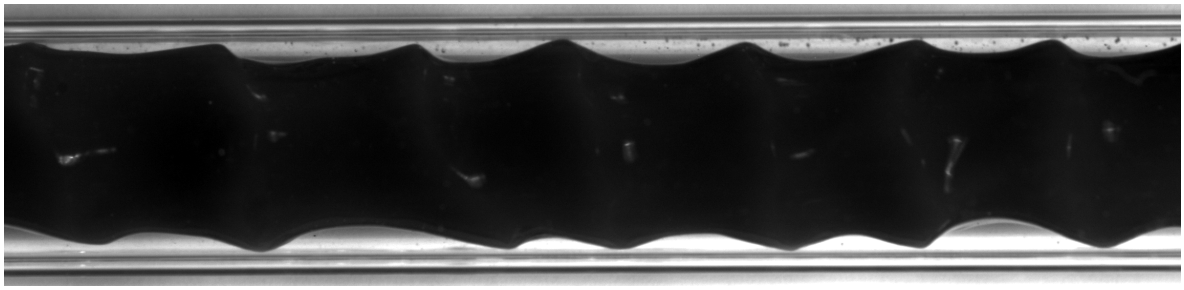

Figure 7.1: Typical core-annular flow pattern for $Q_o = 0.35$ l/s, $C_w = 20\%$ and $\nu_o \approx 2510$ cSt ($T_o \approx 23.4°$C).

Top view

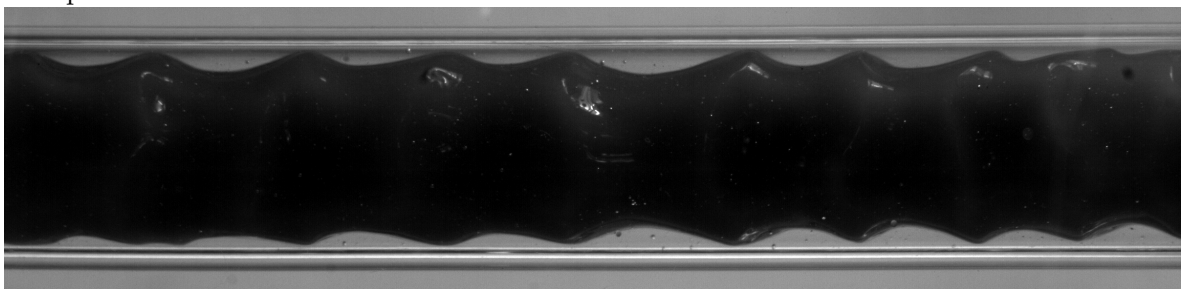

Front view

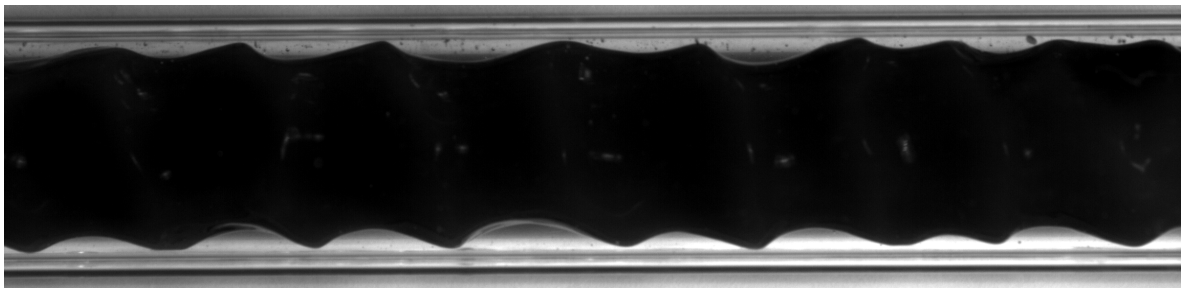

Figure 7.2: Typical core-annular flow pattern for $Q_o = 0.35$ l/s, $C_w = 20\%$ and $\nu_o \approx 1440$ cSt ($T_o \approx 30.3°$C).

Top view

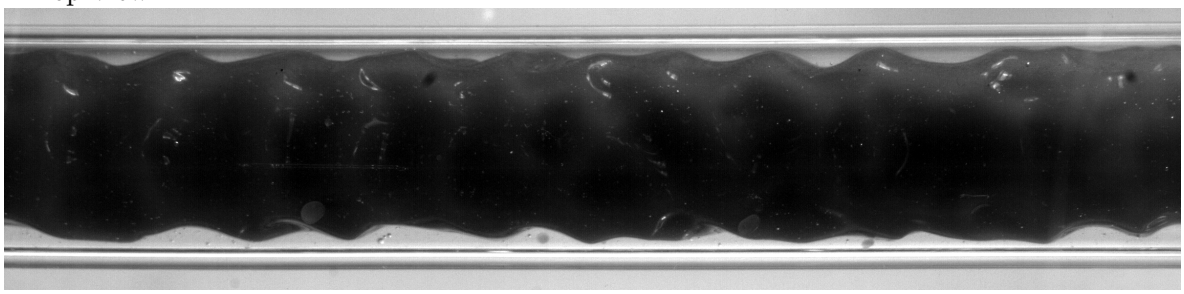

Front view

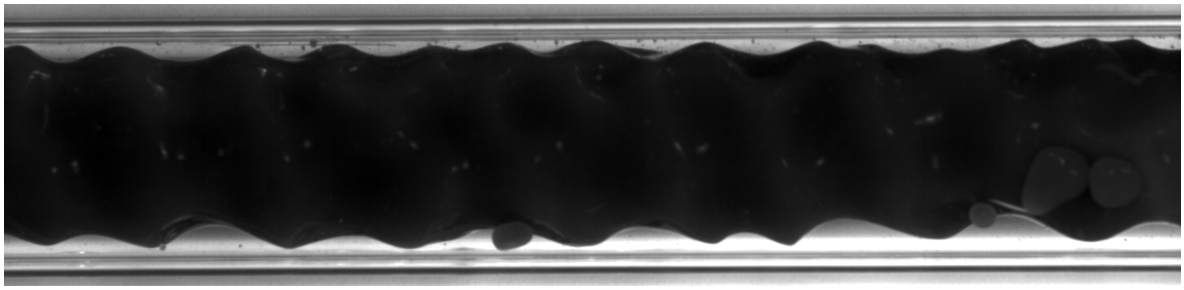

Figure 7.3: Typical core-annular flow pattern for $Q_o = 0.35$ l/s, $C_w = 20\%$ and $\nu_o \approx 760$ cSt ($T_o \approx 39.1°$C).

Top view

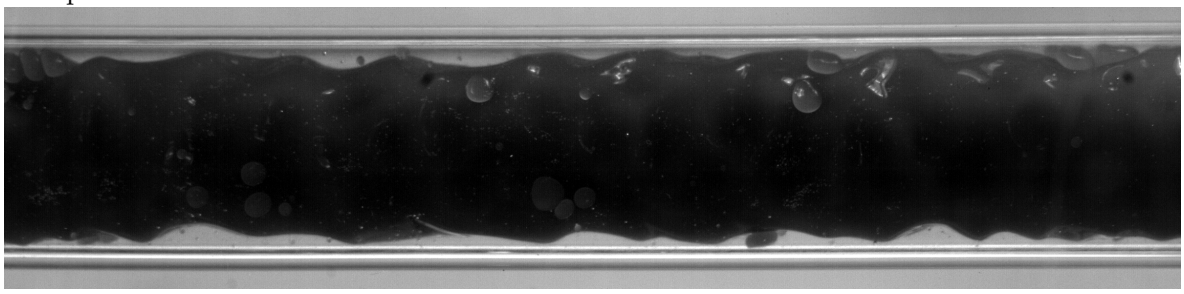

Front view

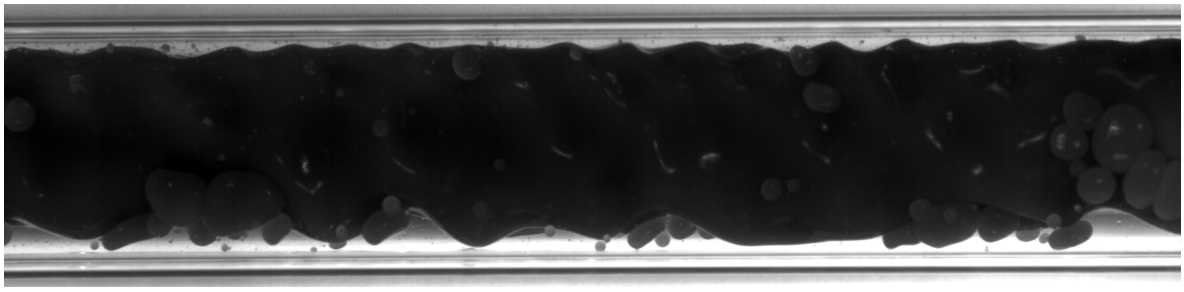

Figure 7.4: Typical core-annular flow pattern for $Q_o = 0.35$ l/s, $C_w = 20\%$ and $\nu_o \approx 440$ cSt ($T_o \approx 47.6°$C).

Top view

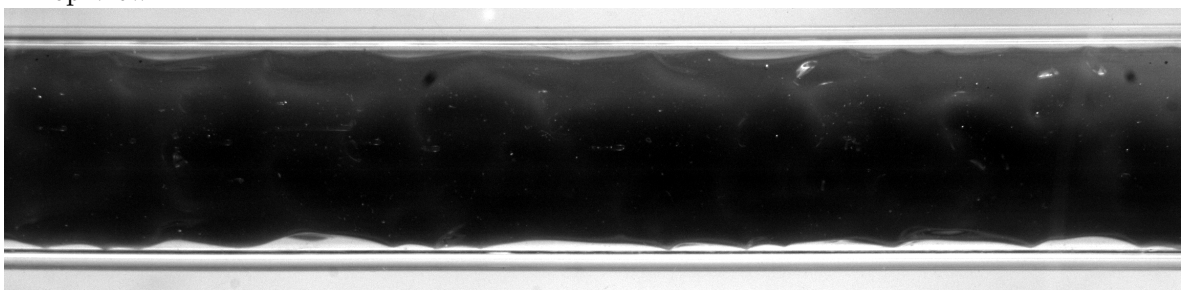

Front view

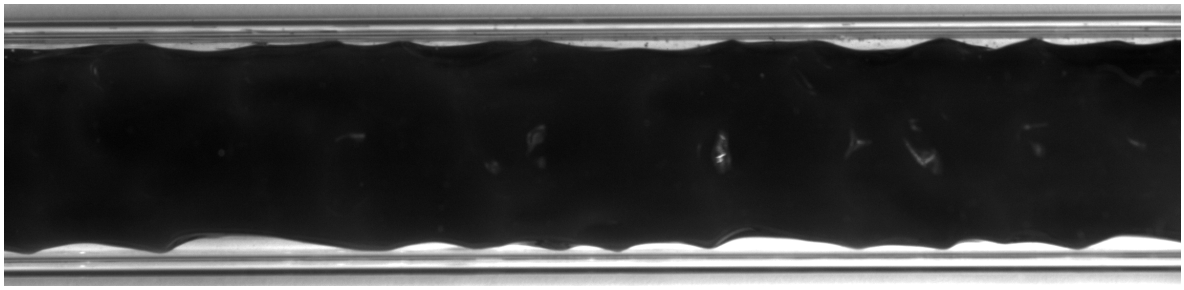

Figure 7.5: Typical core-annular flow pattern for $Q_o = 0.35$ l/s, $C_w = 12\%$ and $\nu_o \approx 2490$ cSt ($T_o \approx 23.5°$C).

Top view

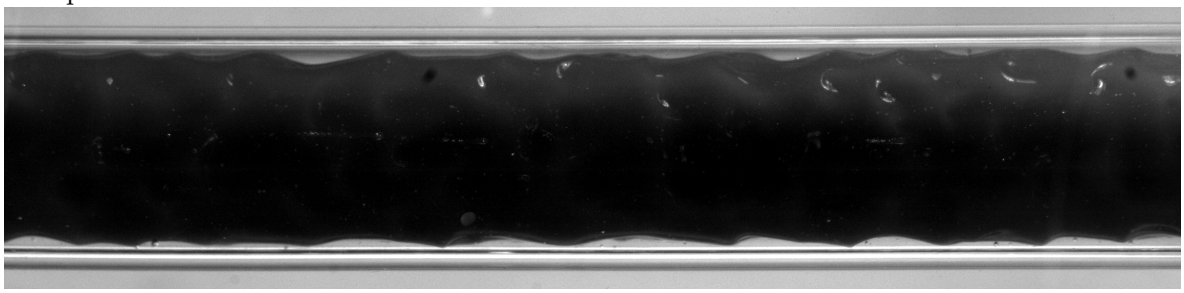

Front view

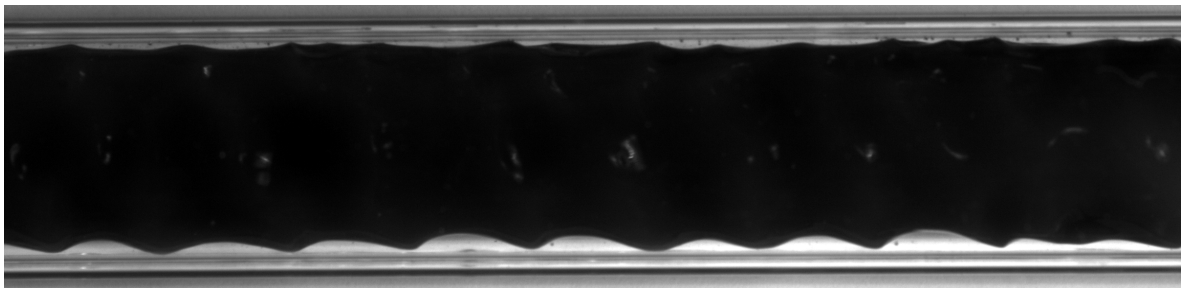

Figure 7.6: Typical core-annular flow pattern for $Q_o = 0.35$ l/s, $C_w = 12\%$ and $\nu_o \approx 1380$ cSt ($T_o \approx 30.8°$C).

Top view

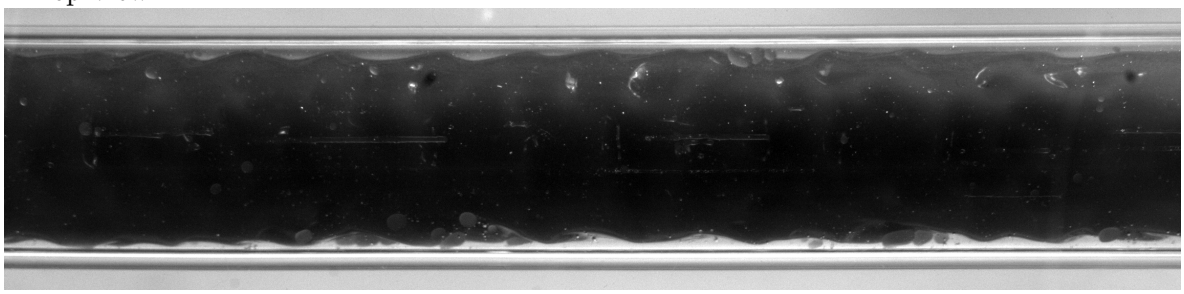

Front view

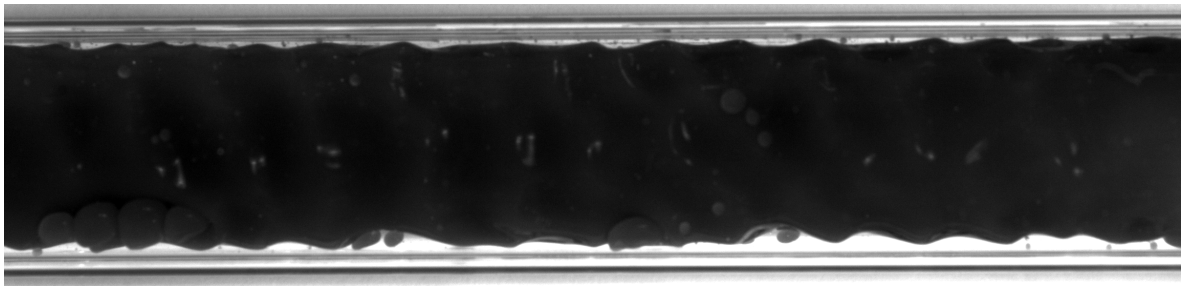

Figure 7.7: Typical core-annular flow pattern for $Q_o = 0.35$ l/s, $C_w = 12\%$ and $\nu_o \approx 780$ cSt ($T_o \approx 38.7°$C).

Top view

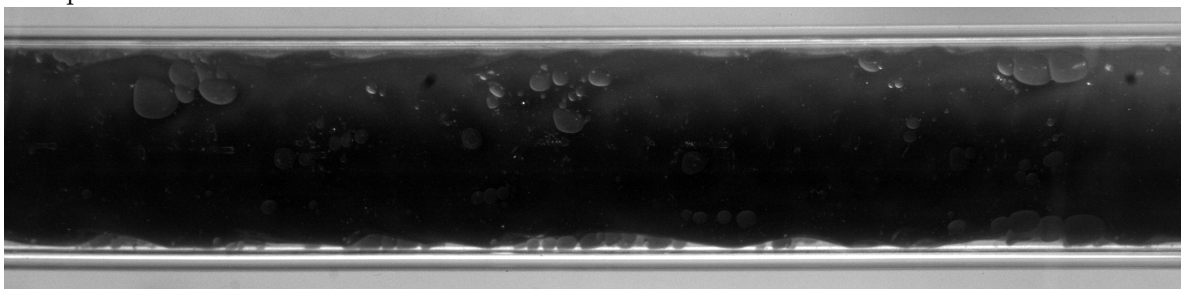

Front view

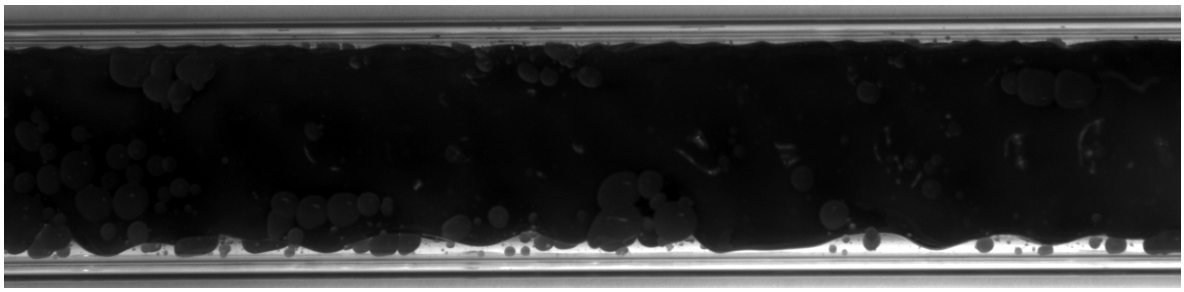

Figure 7.8: Typical core-annular flow pattern for $Q_o = 0.35$ l/s, $C_w = 12\%$ and $\nu_o \approx 420$ cSt ($T_o \approx 48.3°$C).

Chapter 8

Conclusions and Recommendations

8.1 Conclusions

The influence of the oil viscosity on oil-water core-annular flow has been investigated experientially. Several modifications, such as an electronic pressure sensor and a new measurement pipe, were successfully implemented. The experiments were performed for one fixed value of the oil flow rate for which the watercut and oil viscosity were varied. The pressure drop measurements are performed and compared to previous results of Ingen Housz et al. Deviations between the data sets are caused by differences in the oil fluid properties.

The scaled pressure drop as function of the viscosity ratio is presented, from which it is concluded that transport by means of core-annular flow is more beneficial at a high viscosity ratio. Here the measured pressure drop is scaled with calculated pressure drop for single phase oil flowing at the same flow rate and viscosity. At a high viscosity ratio the scaled pressure drop is almost independent of the watercut. At a lower viscosity ratio the amount of water needed to lubricate the oil core causes an increase in the scaled pressure drop and thus the effect of the total throughput becomes more important.

Various scaling parameters are investigated. The Reynolds mixture number based on a weighted averaged viscosity resulted in scalable data. This means that all data point fall on a single straight line when the scaled pressure drop is considered as a function of the mixture Reynolds number. However, the physical interpretation of the mixture viscosity is questionable and requires further investigation.

The measurements are used to test to two different models to predict the pressure drop. The two-fluid model of Brauner under estimates the measured scaled pressure drop by a factor of approximately 3.5. The pseudo fluid model by Bannwart slightly over predicts the measured absolute pressure drop. For a small watercut the deviation between this model and the experiments is larger.

Core-annular flow is visualized using by a high-speed camera. A mirror placed above the imaging section enables the simultaneous recording of the front and top view of the flow. The flow visualisation study shows a clear distinction in the oil-water interface when decreasing the oil viscosity. The waves present on the interface become shorter in length and more irregular when the oil viscosity is decreased. This is found for both large and small watercuts. Furthermore, for decreasing oil viscosity, oil drops are observed in the water annulus. Since the pipe wall is clean after an experiment it can be concluded that oil is still properly lubricated by water in all experiments. In all visualized cases, the shape of the wave shows similarity to the inertia dominated levitation mechanism, which is the 'flying core' model.

The interfacial tension is an important parameter for the stability of core-annular flow. This is experienced first hand using a different type of oil with low interfacial tension; see appendix B for a detailed description.

8.2 Recommendations for further research

Based on the experience of this project, recommendations for further experimental research are given here.

The high-speed camera footage is of good quality for quantitative investigation. The oil-water interface can be tracked to determine the length and amplitude of the waves. Furthermore, the core eccentricity and water hold-up can be estimated.

The water hold-up is an important parameter to quantify and to understand the flow behaviour. It is also important from a modelling perspective and for comparison with numerical simulations. A new sensor to measure the in-situ water fraction can be a topic for further research. From the literature review it is concluded that an impedance sensor based on the conductivity of water is a suitable candidate, e.g. [31]. Sensor rings and points are flush mounted with the wall and cause minor distortion to the flow. In appendix A of the PhD thesis of Belt [32] detailed information is provided on the development, calibration and application of such a conductance sensor.

The combination of high-speed camera images and the conductance sensor can be a valuable combination. The thickness of the annulus can be estimated at four circumferential locations from the images and be used for validation of the conductance sensor. The sensor can measure at a higher spatial resolution which is helpful to detect variations in the wave patterns around the core.

In this study, only one fluid property is investigated in detail: the oil viscosity. Other variations in fluid properties, such as the density difference or interfacial tension, are an interesting approach for further research. The interfacial tension, for example needs to be sufficiently high to maintain a deformable interface.

Experiments with different pipe materials are interesting for two reasons. Firstly, PMMA is a hydrophilic material which might influence the flow. It is also susceptible for oil contact, meaning that when fouling of oil occurs it sticks to the pipe wall. Investigation into pipe coatings to reduce the effect of fouling can be interesting from an industrial application point of view. The roughness of the pipe influences the pressure drop, which can be the result of an applied coating.

Comparing core-annular flow in different pipe diameters is an other interesting approach. For a larger pipe diameter, the core can also have a larger diameter. The buoyant force will increase with a larger core. This might be an interesting approach to verify the scaling properties.

Studying core annular flow in a different geometries, both experimentally and numerically, can be an interesting objective. Different bend radii or an helix-like structure can be of interest. Different geometries can also be in the form of an small obstruction in the pipe or a misaligned fitting. Design codes describe the maximum allowable tolerances. It can be studied whether these tolerances are also applicable for stable core-annular flow.

Flow maps provide an overview of the expected flow regime based on the oil and water superficial velocities. Criteria for transition of one flow regime to the other are made in the literature. The fluid properties, such as the viscosity, play a role in these criteria. Generating flow maps for different values of the viscosity can be used to test the robustness of the transition models.

Implementation of a measurement system with particle image velocimetry (PIV) seems to be a very interesting approach to the topic. No publications have been found where PIV is used to investigate core-annular flow in particular. Quantitative data of the flow field in the turbulent annulus can result in better understanding of the levitation mechanism and can be used for validation of numerical studies.
PIV also seems to be a very challenging approach. The oil is opaque and limits the field of view. The water supply needs modification to inject seeding particles. Water with seeding particles and oil are collected in the separation vessel. A point of concern is the influence of the particles on the oil properties.

8.3 Improvements of the set-up

During the project, a number of limitations of the current set-up are encountered which are briefly discussed below.

Water for the liquid in the annulus is taken directly from the tap, but has a limited flow rate. Having a powerful water supply would reduce fouling at the end of an experiment. The current water flow rate cannot be set to a flow rate equal to the total flow rate used in the core-annular flow experiment. Stratified flow occurs and the flow loop gets fouled. Using a separate water container and pump to increase the water flow rate would be great improvement. It also enables the possibility to control the annular fluid.

A short investigation shows that the water pressure in the tap is capable to reach 0.2 l/s, compared to the 0.11 achieved currently. The connecting tubes, water flow meter and/or the connection to the divider impose a large pressure drop on the water supply that limits the water flow rate. It highly recommended to investigate these parts as well when upgrading the water supply.

An other point of improvement are the PVC pipe sections of the flow loop. The first 2 m long pipe and the bends contain scratches on the inside surface, which can affect the measurements. Also, the first 2 m long straight section is slightly bended.

A last point of concern is the connection between the end of the flow loop and the separation vessel. This is flexible hose, situated higher than the flow loop itself. This means that the outlet is pressurized. It is assumed that the measured pressure drop remains unaffected by this.

Bibliography

[1] Joseph, D.D. and Renardy, Y.Y. *Fundamentals of Two-Fluid Dynamics, Part I: Mathematical Theory and Applications*. Interdisciplinary Applied Mathematics. Springer-Verlag, 1993.

[2] Joseph, D.D. and Renardy, Y.Y. *Fundamentals of Two-Fluid Dynamics, Part II: Lubricated Transport, Drops and Miscible Liquids*. Interdisciplinary Applied Mathematics. Springer-Verlag, 1993.

[3] Brauner, N. Modeling and control of two phase flow phenomena: liquid–liquid two phase flow systems. *School of Engineering, Tel-Aviv University, Israel*, 2002.

[4] Guevara, E., Gonzalez, J. and Nuñez, G. Highly viscous oil transportation methods in the venezuela industry. In *Proceeding of the 15th World Petroleum Congress*, pages 495–502, 1998.

[5] Shi, J. *A study on high-viscosity oil-water two-phase flow in horizotal pipes*. PhD thesis, Cranfield University, 2015.

[6] Bratland, O. *Pipe Flow 2: Multi-phase Flow Assurance*. www.drbratland.com, 2010. ISBN 978-616-335-926-1.

[7] Arney, M.S., Bai, R., Guevara, E., Joseph, D.D. and Liu, K. Friction factor and holdup studies for lubricated pipelining–I, Experiments and correlations. *International Journal of Multiphase Flow*, 19(6):1061–1076, 1993.

[8] Ooms, G., Segal, A., van der Wees, A.J., Meerhoff, R. and Oliemans, R.V.A. A theoretical model for core-annular flow of a very viscous oil core and a water annulus through a horizontal pipe. *International Journal of Multiphase Flow*, 10(1):41–60, 1983.

[9] Oliemans, R.V.A., Ooms, G., Wu, H.L. and Duijvestijn, A. Core-annular oil/water flow: the turbulent-lubricating-film model and measurements in a 5 cm pipe loop. *International Journal of Multiphase Flow*, 13(1):23–31, 1987.

[10] Joseph, D.D., Bai, R., Chen, K.P. and Renardy, Y.Y. Core-annular flows. *Annual Review of Fluid Mechanics*, 29(1):65–90, 1997.

[11] Ooms, G., Pourquie, M.J.B.M. and Beerens, J.C. On the levitation force in horizontal core-annular flow with a large viscosity ratio and small density ratio. *Physics of Fluids*, 25(3):032102, 2013.

[12] Brauner, N. Liquid-liquid two-phase flow systems. In *Modelling and Experimentation in Two-Phase Flow*, pages 221–279. Springer, 2003.

[13] Bannwart, A.C. Modeling aspects of oil–water core–annular flows. *Journal of Petroleum Science and Engineering*, 32(2):127–143, 2001.

[14] Ghosh, S., Mandal, T.K., Das, G. and Das, P.K. Review of oil water core annular flow. *Renewable and Sustainable Energy Reviews*, 13(8):1957–1965, 2009.

[15] Shi, J. and Yeung, H. Characterization of liquid-liquid flows in horizontal pipes. *AIChE Journal*, 63(3):1132–1143, 2017.

[16] Grassi, B., Strazza, D. and Poesio, P. Experimental validation of theoretical models in two-phase high-viscosity ratio liquid–liquid flows in horizontal and slightly inclined pipes. *International Journal of Multiphase Flow*, 34(10):950–965, 2008.

[17] *Morlina S2 B 680*. Dutch Royal Shell, 2012. Dutch version available on: `epc.shell.com`, English version from: `http://www.gerlub-schmierstoffe.de/fileadmin/pdf/datenblaetter/industrie/Maschinen%C3%B6le/PI/Shell%20Morlina%20S2%20B%20680.pdf`, Accesed: June 20, 2017.

[18] Viscosity and density of water, Viscopedia: A free encyclopedia for viscosity. URL: `http://www.viscopedia.com/viscosity-tables/substances/water/`, 2008. Acessed: June 20, 2017.

[19] *Krüss Digital Tensiometer K9*, 2001. Manual available at Shell Laboratory Amsterdam.

[20] Harkins, W.D. and Jordan, H.F. A method for the determination of surface and interfacial tension from the maximum pull on a ring. *Journal of the American Chemical Society*, 52(5):1751–1772, 1930.

[21] Zuidema, H.H. and Waters, G.W. Ring method for the determination of interfacial tension. *Industrial & Engineering Chemistry Analytical Edition*, 13(5):312–313, 1941.

[22] Peters, F. and Arabali, D. Interfacial tension between oil and water measured with a modified contour method. *Colloids and Surfaces A: Physicochemical and Engineering Aspects*, 426:1–5, 2013.

[23] Flock, D.L., Le, T.H. and Gibeau, J.P. The effect of temperature on the interfacial tension of heavy crude oils using the pendent drop apparatus. *Journal of Canadian Petroleum Technology*, 25(2), 1986.

[24] Ingen Housz, E.M.R.M. Core-Annular Flow: Experimental and numerical studies on core-annular flow through a horizontal pipe. Master's thesis, Delft University of Technology, 2016.

[25] *General Operating Instructions, Validyne Variable Reluctance Pressure Transducer*. Validyne Engineering. Manual available at TU Delft.

[26] *Testing the DP15 for functionality*. Validyne Engineering, 2013. `https://www.youtube.com/watch?v=wQZSErTvh9U`.

[27] *CD15 Instructional Video.* Validyne Engineering, 2013. `https://www.youtube.com/watch?v=ODFO_IBT-mo`.

[28] Radhakrishnan, R. The effects of viscosity on core-annular flow: Numerical simulations and experiments for core-annular flow. Master's thesis, Delft University of Technology, 2016.

[29] Ingen Housz, E.M.R.M., Ooms, G., Henkes, R.A.W.M., Pourquie, M.J.B.M., Kidess, A. and Radhakrishnan, R. A comparison between numerical predictions and experimental results for core-annular flow with a turbulent annulus. *International Journal of Multiphase Flow*, 95:271 – 282, 2017.

[30] Einstein, A. Eine neue bestimmung der moleküldimensionen. *Annalen der Physik*, 324 (2):289–306, 1906.

[31] Coney, M.W.E. The theory and application of conductance probes for the measurement of liquid film thickness in two-phase flow. *Journal of Physics E: Scientific Instruments*, 6(9):903–910, 1973.

[32] Belt, R.J. *On the liquid film in inclined annular flow.* PhD thesis, Delft University of Technology, 2007.

Appendix A

Technical Data Sheet Morlina S2 B 680

English version of the technical data sheet of *Morlina S2 B 680* provided by its manufacture *Dutch Royal Shell* [17].

Technical Data Sheet

Previous Name: **Shell Morlina Oil**

Shell **Morlina** *S2 B 680*

- *Reliable Protection*
- *Industrial Application*
- *Water Shedding*

Industrial Bearing and Circulating Oils

Shell Morlina S2 B oils are high performance oils designed to provide outstanding oxidation and water separation protection for most general industrial bearing and circulating oil system applications and certain other industrial applications which do not require oils with extreme pressure (EP) properties. These oils meet the requirements of the Morgan Construction Company and Danieli for common bearing oils.

DESIGNED TO MEET CHALLENGES

Performance, Features & Benefits

- **Long oil life - maintenance saving**
  Shell Morlina S2 B oils are formulated with a well proven rust and oxidation inhibitor additive package that helps provide consistent performance and protection throughout the maintenance interval.
- **Reliable wear and corrosion protection**
  Shell Morlina S2 B oils help prolong the life of bearings and circulating systems through:

  -Excellent water separation characteristics that helps ensure that critical oil films are retained between highly loaded parts.

  -Good air release characteristics to minimize cavitation and associated damage to circulating pumps.

  -Helps protect against corrosion, oxidation, and emulsion formation, even in the presence of water.
- **Maintaining system efficiency**
  Shell Morlina S2 B oils are blended with high quality, solvent refined base oils that promote good water separation and air release to ensure the efficient lubrication of the machines and systems.

Main Applications

- **Machine circulation system**
- **Oil lubricated bearings**
  Suitable for most plain and rolling element bearings and general industrial applications.
- **Roll-neck bearings**
- **Enclosed industrial gear systems**
  Low or moderately loaded enclosed gears where EP performance is not required.

Specifications, Approvals & Recommendations

- Morgan "Morgoil®" Lubricant Specification New Oil (Rev. 1.1) (MORGOIL is a registered trademark of the Morgan Construction Company)
- Danieli Standard Oil 6.124249F
- DIN 51517-1 – type C
- DIN 51517-2 – type CL

  For a full listing of equipment approvals and recommendations, please consult your local Shell Technical Help Desk, or the OEM Approvals website.

Compatibility & Miscibility

- **Paint Compatibility**
  Shell Morlina S2 B oils are compatible with seal materials and paints normally specified for use with mineral oils.

Typical Physical Characteristics

Properties			Method	Shell Morlina S2 B 680
ISO Viscosity Grade				680
Kinematic Viscosity	@40°C	mm^2/s	ASTM D445	680
Kinematic Viscosity	@100°C	mm^2/s	ASTM D445	37
Density	@15°C	kg/m^3	ISO 12185	910
Viscosity Index			ISO 2909	min 85
Flash Point (COC)		°C	ISO 2592	300
Pour Point		°C	ISO 3016	-9
Rust, Distilled Water			ASTM D665 A	Pass
Emulsion Test - @82°C (Unless specified by *)		Mins	ASTM D1401	min 40
Oxidation Control Test : TOST		Hrs	ASTM D943	min 1000
Oxidation Control Test : RBOT		Mins	ASTM 2272	min 300
Foam Test, Seq II		ml foam at 0/10 mins	ASTM D892	20/0

These characteristics are typical of current production. Whilst future production will conform to Shell's specification, variations in these characteristics may occur. *@54°C

Health, Safety & Environment

- **Health and Safety**

  Shell Morlina S2 B is unlikely to present any significant health or safety hazard when properly used in the recommended application and good standards of personal hygiene are maintained.

  Avoid contact with skin. Use impervious gloves with used oil. After skin contact, wash immediately with soap and water.

  Guidance on Health and Safety is available on the appropriate Material Safety Data Sheet, which can be obtained from your Shell representative.

- **Protect the Environment**

  Take used oil to an authorised collection point. Do not discharge into drains, soil or water.

Additional Information

- **Advice**

  Advice on applications not covered here may be obtained from your Shell representative.

Technical Data Sheet

Viscosity - Temperature Diagram for Shell Morlina S2 B

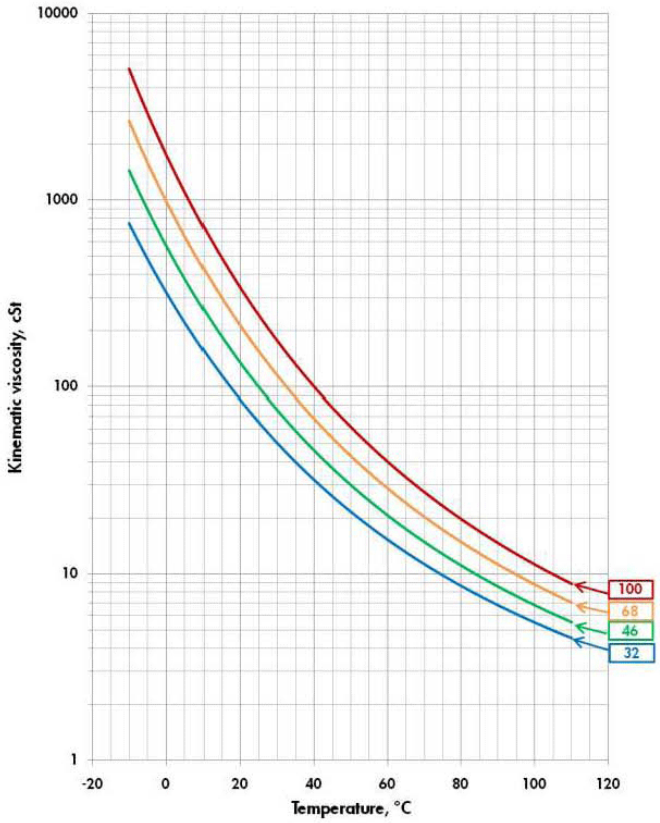

Shell Lubricants

Page 3 of 4

20/08/2012

Viscosity - Temperature Diagram for Shell Morlina S2 B

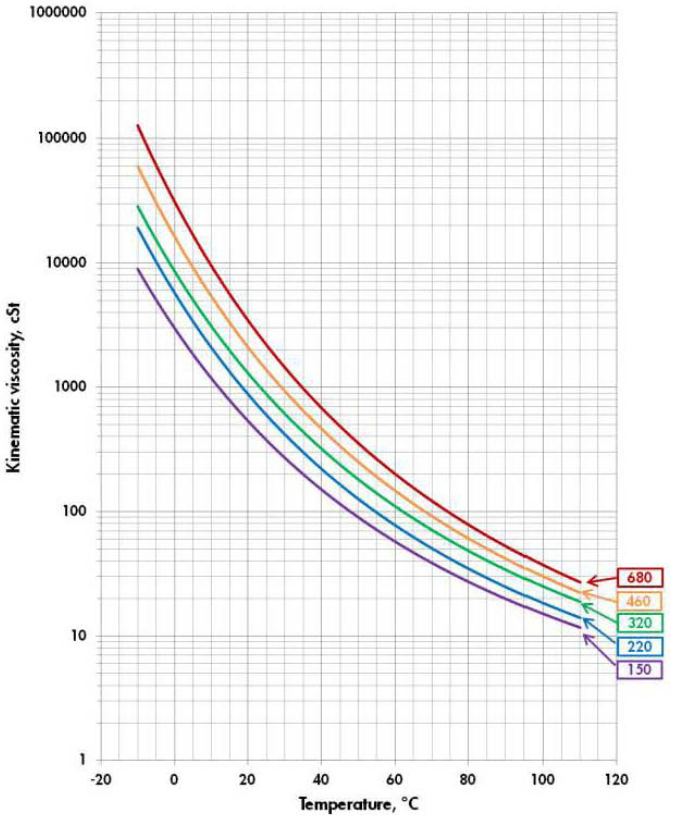

Shell Lubricants

Page 4 of 4

20/08/2012

Appendix B

Encountered Experimental Problems

During the start of the experimental campaign, several problems were encountered. Some were easily solved, whereas others proved to be a real challenge to determine the cause. Two major problems are described in this appendix.

B.1 New oil

As explained in section 4.7, the oil needed to be replaced since its properties had changed over time. Mainly the viscosity of the oil has decreased significantly. However, the used oil, *Morlina S4 B 680*, was not available any more. A substitute oil, *Cassida GL 680*, was chosen based on similar properties for viscosity and density, see table B.1.

Table B.1: Book values of the fluid properties for the old oil, *Morlina S4 B 680*, and the new oil, *Cassida GL 680*.

Property		Morlina S4 B 680		Cassida GL 680	
Kin. viscosity	at 40 °C	680	cSt	680	cSt
	at 100 °C	61.9	cSt	58.6	cSt
Density	at 15 °C	857	kg/m^{-3}	858	kg/m^{-3}

The first experiment with the Cassida oil was promising and core-annular flow was observed clearly. The pipe wall was fouled after the experiment, but this has happened when the experiment was stopped.

In the experiments that were carried out later, core-annular flow was observed for a brief period after starting the oil flow. A clear transparent layer of water surrounded the core. Before fully developed core-annular flow was obtained, the oil has touched the pipe wall. This was unexpected since core-annular flow was achieved with the Morlina oil.

It was also observed that the oil has changed colour from transparent to milky-white after it has been brought in contact with water in the separation vessel. A photograph of the two samples is given in figure B.1. A change in colour was also observed for the Morlina oil, therefore it could not immediately be concluded that the Cassida oil was causing the failure of the core-annular flow.

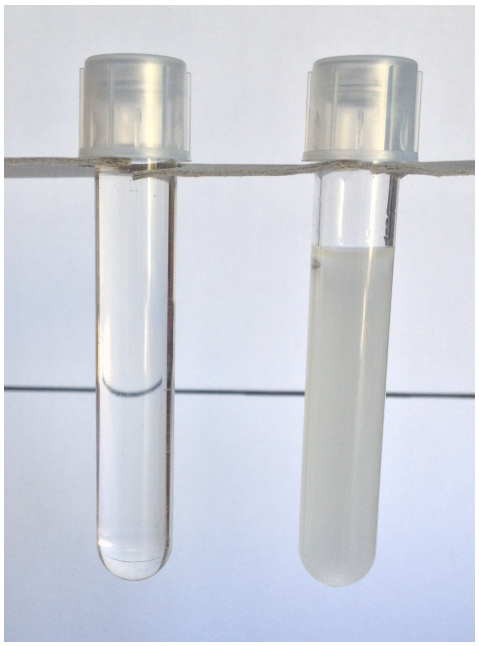

Figure B.1: Photograph of the clean (left) and contaminated (right) Cassida oil. The black line on the background indicates the transparency of the clean oil sample.

B.1.1 Root cause analysis

The failure of the oil to reproduce core-annular flow could be due to various causes, such as fouled pipe walls, misaligned connections of the re-attachable links, the flow conditions or the fluid properties itself. A systematic approach is required to find the root cause of the problem. The list below summarizes the actions taken to determine if the cause is in the set-up; however non of these actions resulted in core-annular flow.

- All pipe segments are thoroughly cleaned to remove possible oil contamination. A possible roughness element, such as remaining oil, can disrupt the water annulus such that the oil core touches the pipe wall with the initiation of fouling.
- The re-attachable links are connected with utmost care to ensure a smooth inner pipe connection surface. Again, a roughness element could lead to fouling.
- Different flow conditions are set. Based on a flow map by Grassi et al. [16] it was concluded that the flow conditions were well inside the stable regime for core-annular flow. Also maximum flow conditions are tried.

At the end of an experiment the oil flow rate is stopped and the water flow rate is set to maximum to flush out as much oil as possible. Since the water flow rate can not be set to the total flow rate of the experiment, core-annular flow can not be maintained and stratified flow occurs. Waves are present at the oil-water interface in the stratified flow conditions. At the end of the experiments performed with the Morlina oil, similar flow structures were noticed. The pipe wall, however, did remain much cleaner for the Morlina oil, where fouling only occurred near the links. Another observation concerns the behaviour of the waves when the experiment is stopped. For the Morlina oil the waves on the interface moved almost stationary with the flow, whereas for the Cassida oil the wave pattern was much more chaotic and the waves on the interface were 'dancing' as they moved downstream with the flow. This could be an indication that the instability of core-annular flow is caused by the oil properties.

B.1.2 Checking the oil properties

As mentioned before, the oil has changed colour after being in contact with water. To exclude the possibility that the oil is causing the instability, its properties are measured again. The procedure to measure the density, viscosity and interfacial tension are described in chapter 3 *Fluid Properties*. An overview of the measured properties is given at the end of this section in table B.2

Firstly, the viscosity is checked. Comparison of the two samples did not show a significant difference.

With logic reasoning it was concluded that the oil density could have increased over time or remained similar. Since the oil was in contact with water, it has changed colour. Therefore, water could have been absorbed by the oil leading to the change in colour. So, when water is absorbed, it will be more dense than the clean oil. This would result in a smaller density difference between the oil and water and therefore the buoyancy force acting on the core is smaller. This has a stabilizing effect on core-annular flow and could thus not significantly affect the flow.

The density of both samples has been measured, and an almost similar value was found.

After discussion with Ben Norder of *Applied Physisc*, who performed the viscosity measurements, an other attempt was made to explain why the oil has changed colour. At that time, the density has not yet been measured and it was still assumed that absorption of water caused the change in colour. An oil sample is put into a vacuum stove to vaporize any possibly absorbed water. The oil sample remained milky white in colour and the weight of the sample was unchanged. It was concluded that the change in colour is due to an irreversible chemical reaction between the oil and water.

Manufactures of lubrication oils, such as both oils, add certain additives to their product to enhance its performance under versatile conditions. A small amount of water near a gear, for example, can cause damage and needs to be encapsulated by the oil. The exact type of additives is company secret and is not specified on the technical data sheet.

The interfacial tension could be the fluid property which caused break down of the core-annular flow. However, it is not possible to measure this quantity at the university itself. Measurements of the interfacial tension with a ring tensiometer, obtained under supervision of Menno van Dijk at the Shell laboratory in Amsterdam, provided insight in the problem. The Cassida oil has an interfacial tension which is about a factor 10 smaller than the Morlina oil.

The value of the interfacial tension is hard to measure with the ring tensiometer, since it can only display to an accuracy 0.1 mN/m accurately. A small movement of the ring through the interface already generates an increase of the value by 0.5 mN/m after which is settles at a lower value. Using the ring tensiometer for this oil might not be the most accurate technique, but it gives an indication of the order.

It must be noted that the interfacial tension is measured after five minutes of settling time of the interface. This explains why the clean and contaminated Cassida oil samples have almost similar interfacial tension. Still core-annular flow was observed with uncontaminated oil in the first experiment. This can be explained by the short residence time of the flow during an experiment. In approximately eight seconds, the flow goes from the divider to the separation vessel and the additives have not had the time to react fully with water.

B.1.3 Newer oil: *Morlina S2 B 680*

At the moment that the decision was made to order a new batch of oil, the interfacial tension had not yet been measured. Although from the actions performed in the set-up for the flow behaviour it was concluded that the oil itself was the cause of the failure to give core-annular flow. An oil from the same product line as the old oil was chosen, *Morlina S2 B 680*. Since the interfacial tension is not specified by the manufacturer this still provided a risk. The second experiment, i.e. after long contact with water in the separation vessel, proved to be the real test. Fortunately it passed with flying colours.

B.1.4 Conclusion

With systematic investigation, the cause of the instability of the core-annular flow was brought back to the properties of the oil. The density and viscosity were not affected although the colour had changed. The measurement of the interfacial tension showed that the value for the Cassida oil is significantly lower than for the previously used Morlina oil. As mentioned by Bannwart [13], the interface must have a certain elasticity such that it can sustain deformations in the flow. When the interfacial tension is too low, the hydrodynamic forces cause rupture of the interface and water mixes with the oil causing an emulsion. It can thus be concluded that the interfacial tension plays a crucial role in the stability of core-annular flow.

To finalize, all measured oil properties at 20 °C of the old oil, *Morlina S4 B680*, the new oil, *Cassida GL 680*, and the final new oil, *Morlina S2 B 680*, are given in table B.2.

Table B.2: Overview of the measured oil properties of *Morlina S4 B 680* [24], *Cassida GL 680* (Clean & contaminated) and *Morlina S2 B 680* (see also chapter 3). All properties are at 20 °C.

Oil		Density [kg/m^3]	Dyn. viscosity [Pa·s]	Interfacial tension [mN/m]
Morlina S4 B 680	Measured by [24]	855	2.32	16
Cassida GL 680	Clean	853	2.04	2.2
	Contaminated	853	2.04	1.4
Morlina S2 B 680	New	913	3.05	13.8

B.2 Pressure measurements

The new oil, *Molrina S2 B 680*, was inserted in the set-up and core-annular flow was observed. A first step in the experimental campaign was to reproduce experimental data as reported in the master thesis of Ingen Housz [24]. Furthermore, equal experimental conditions are repeated to test the reproducibility of the measured pressure drop with the new pressure sensor. The flow conditions are at room temperature with a fixed oil flow rate of 0.35 l/s and varying watercut.

Figure B.2 shows the measured pressure drop for core-annular flow as function of the watercut. The data of Ingen Housz at this oil flow rate is included for reference. There is a clear deviation between the results. The minimum in the pressure drop around 12% watercut is not observed in the new measurements. Overall, our measurements are significantly lower and

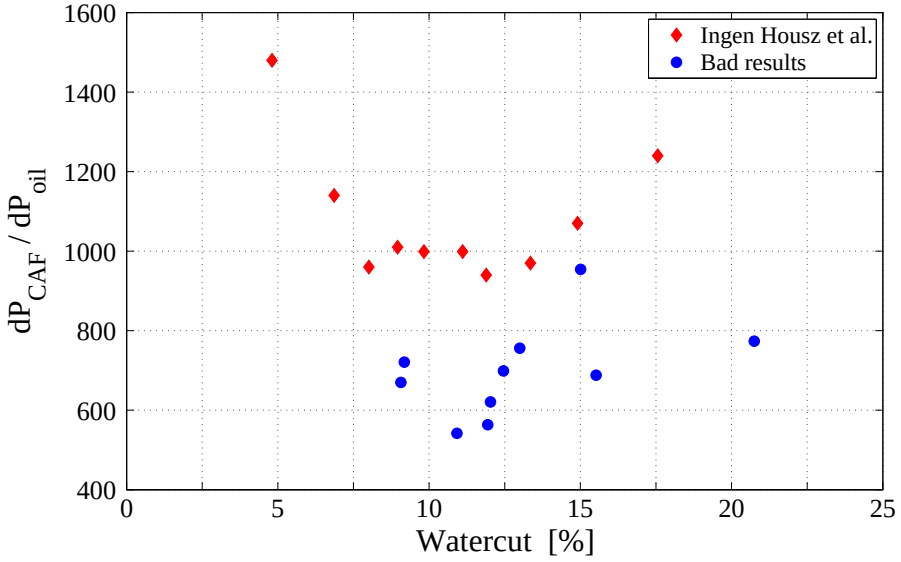

Figure B.2: First data of the measured pressure drop as function of the watercut. Previous obtained data [24] at equal oil flow rate of 0.35 l/s are included for reference.

the reproducibility between (almost) equal flow conditions is poor. The estimated uncertainty of the pressure measurements is approximately 80 Pa.

B.2.1 Trouble shooting of the pressure measurements

Possible explanations of the deviations between the measurements can be:

- New oil with larger viscosity and smaller density difference.
- New measurement pipe.
- Other pressure sensor (inverted U-tube compared to electronic pressure sensor).

The pressure sensor itself has been tested for correct working and its correct calibration. Special care is taken when venting the sensor, such that air bubbles are not present in the sensor and the connected tubing. The sensor itself is placed at the table and variations in height of the sensor with respect to the flow loop are excluded.

The oil itself could not cause the large deviations between our measurements. A similar trend, forming a minimum in pressure drop, must be present. This assumption is confirmed in the literature, both theoretically, e.g. [13, 12] and experimentally e.g. [24]. The new oil could cause the overall pressure drop measurements to be lower. The smaller density difference leads to a less eccentric position of the core and additional friction due to eccentricity is reduced [12].

B.2.2 Pressure holes

During the experiments fouling was observed at the pressure points, especially at the upstream pressure hole. When the a pressure tap is sealed with oil, the pressure measurements are corrupted.

With the new measurement pipe, the points for pressure measurements are redesigned. It is now possible to have clear optical access to the pressure tap. It is also possible to adjust the height of tube connected to the sensor. Special care is taken to obtain flush alignment of the tube with the pipe wall. However, fouling remained present near the pressure hole.

The holes are located at the bottom of the pipe and therefore it is unlikely that the fouling occurred when the experiment is stopped. Different approaches to stop the experiment more gently did not fix the fouling problem.

Close inspection of the pressure holes proved to give the answer. Small burrs from drilling were still present at the both holes. At the upstream hole, a large burr was hanging over the pressure hole, almost sealing it from the flow. A photograph is given in figure B.3. The flow direction is from left to right and the brown colour is oil which has fouled the pipe wall.

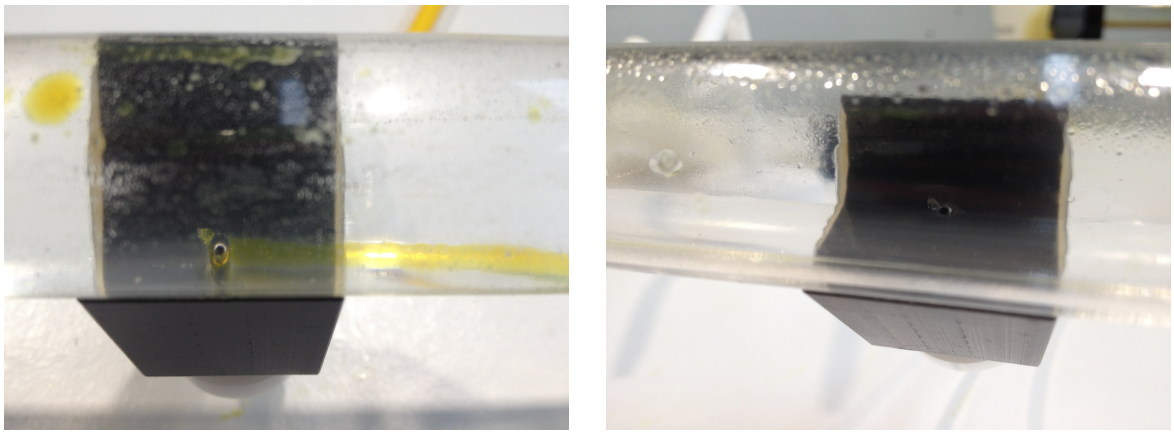

Figure B.3: Photographs of the upstream pressure hole with the burr. *Left*: After experiment, where fouling is present. *Right*: After cleaning.

B.2.3 Solving the problem

The small metal tube connected to the pressure sensor was removed from the connector and a metal wire is used to peal all burrs from the inside of the pipe. This is done with care to prevent scratching the inside pipe wall. It turned out that this caused the unexpected behaviour in the pressure measurements. All results presented in chapter 6 are obtained after the burr was removed.

Appendix C

Operation Protocol for Core-Annular Flow Expiriments

The following document is created to instruct future users on the operation of the experimental set-up.

Protocol Core-Annular Flow Experiment

This protocol entails detailed information on the operation of the *Core Annular Flow* setup.

This protocol is based on one experiment for the total available oil in the oil storage container. That means one experiment per day.

In general, work in a clean environment. This will result in better results and makes it easier to spot possible leaks or other problems.

1. Safety

The setup is located at Process and Energy of the TU Delft. Always follow the safety instructions and indications from the staff.
To enter the platform, and thus to access the setup, it is required to wear safety helmets, safety glasses and safety shoes at all time. If desired, lab coats are available at the setup.

2. Preparation

To prepare the set-up for an experiment, the following actions and check need to be done.

Note: Separation time of oil and water is approximately 22 hours. This is the time between the end of the previous experiment (the day before) and the start of action 6.

1. Check the dump barrel before ascending the platform:
    a. Maximum fluid level: approx. 930 litre
        i. If the barrel is full, contact the lab supervisor and assist with replacement
        ii. Pay extra attention when disposing water when close to maximum level.
    b. Connection valves:
        i. Valve on barrel must be open
        ii. Central de-water valve is switched to dump barrel
2. Switch on power supply of the *Validyne* pressure transducer
    a. The electronics in the power supply needs to warm for about 30 minutes prior to measurements. 'Cold' electronics will cause a drift in the signal.
3. Open main water supply valve
4. Plug in boiler to heat up water for cleaning. Only use the indicated power socket
5. Power on computer and run the LabVIEW VI
    a. Check for errors and act accordingly
6. Check oil level in oil storage container
    a. If the level is below the indicated maximum, pump over oil from the separation vessel to the oil container using the small oil pump
    b. This process takes approximately 20 minutes when the oil level was close to the minimum

7. Only after action 6 is fully completed:
   Check level indicator of the separation vessel
   a. The minimum fluid level is indicated
   b. Dispose excess water from the separation vessel using the valve near the bottom.
   c. The minimum fluid level may not be exceeded!
   d. Monitor the level indicator in LabVIEW for maximum fluid level of the dump barrel.
8. When the boiler is ready (red light turns off)
   a. Fill the rinsing tank to approximately 25 litres
   b. Heat up a second batch of hot water.
9. Connect all pipes of the flow loop, starting from the divider
   a. Take care for flush alignment of the re-attachable links
   b. If necessary, adjust the measurement pipe accordingly
   c. Make sure the pressure taps are at the bottom (or if the visualisation section is in plane with the camera)
   d. Clean the connections with paper towels, if necessary

   Note: If the pipes are not cleaned after a previous experiment, follow the cleaning procedure prior to the experiment. See section 4.
10. Check for horizontal alignment of the flow loop and adjust accordingly
11. Check flush alignment of the metal pressure taps.
    a. This is easier when the pipe is empty
12. Fully open the water tap to the experiment, located at the back of the set-up
13. Optional: Heating up the oil.
    Only after action 6 is fully completed.
    a. Turn on the *Julabo* heating device
       i. Use the arrows to adjust the setting temperature and press 'OK'.
          About 20 °C above the desired oil temperature is good.
          But never above 80 °C
       ii. The internal temperature is the temperature of the heating basin
       iii. The external temperature indicates the temperature of the oil
    b. Set the oil valve at the main oil pump to circulation
    c. Turn on the oil pump at maximum flow rate for circulation (on the front side)
    d. Turn on the heating device by pressing 'OK'
       i. After about 5 seconds, the heating indicator turns on (top left of the display)
       ii. If it keeps flashing, adjust the temperature with the arrows and confirm with 'OK'
    e. From experience is learnt that the measured oil temperature is lower than displayed by the external temperature. This ranges from 0.5 °C to 1.5 °C, depending on the final temperature.
    f. When the oil temperature is approximately 0.5 °C before the final temperature:
       i. Turn off the heating device by pressing 'OK'
       ii. Let oil pump turned on for circulation
    g. When the desired temperature is reached: turn off the oil pump

3. Experiment

Before the experiment, the pressure sensor needs to be calibrated by a zero pressure measurement.

Zero Measurement

14. Unplug the boiler, to avoid power surges during the measurements
15. Double check if all connections are closed
16. Start LabVIEW for monitoring purpose
17. Start the water flow by opening the tap op the divider
    a. Make sure the pipe will be fully filled with water
    b. Run water for approximately 1 minute and meanwhile perform action 18
18. Connect the differential pressure transducer to the pressure connectors
    a. Use the bleed screws on the pressure transducer to remove all air bubbles in the pressure lines!
19. Close the water flow
    a. Make sure no large air bubble are present directly above the pressure holes.
20. Stop LabVIEW and name the output file appropriately
    a. For example: the date + zero as “YYMMDD_ZERO.lvm”
21. Turn off the oil pump (If heating up the oil is required)
22. Start LabVIEW for a ‘zero’ measurement of approximately 40 seconds.
23. Stop LabVIEW data acquisition

Core-annular flow Experiment

24. Calculate the flow conditions using the excel sheet: “Measurements CAF” and create a new entry in the log
25. Name the output file appropriately
    a. For example: “YYMMDD_CAF_1.lvm” for the first experiment of that day.
26. 1) For oil at room temperature:
    a. Set the valve after the oil pump to circulation
    b. Turn on the oil pump to maximum flow rate for 1 minute
    c. Turn of oil pump
    d. Switch oil valve to experiment setting

26. 2) For heated oil:
    a. Check the temperature of the oil and act accordingly to action 13
    b. Stop the oil pump, if applicable on 26. 2) a
    c. Switch the oil valve to experiment setting.
27. Pre-set the oil pump to the calculated setting by rotating the knob
28. Start LabVIEW data acquisition for monitoring
29. Start the water flow rate and set to maximum flow rate for approximately 10 to 30 seconds, depending on the amount of air bubbles
30. Decrease the water flow rate to the calculated setting
31. Start the oil flow by:
    a. First opening the oil supply valve prior to the divider
    b. Start the oil pump

32. Monitor the experiment!
    a. With LabVIEW
    b. Examine the flow by eye
    c. Continuously check the oil level in the oil storage tank.
33. After approximately 80 seconds at an oil flow rate of 0.35 l/s, the oil level is at the minimum level
34. End of the experiment:
    a. Decrease oil flow rate to zero by rotating the knob and simultaneously increase the water flow rate to its maximum
    b. Stop the oil pump when at zero and close the oil supply valve
    c. Run water flow for 1 to 2 min. and check fluid level in separation vessel
    d. Adjust water flow rate to minimize oil droplets. This reduces fouling
    e. Close water flow
    f. Stop LabVIEW data acquisition

4. Cleaning

35. Plug back in the boiler
36. Disconnect the flow loop
37. Put a cup under the outlet of the divider to collect oil
38. Attach the rinsing hoses and connect the flow loop
39. First rinse:
    a. Set the rinsing system to open circuit, using the 3-way valve near the water tank
    b. Use the centrifugal pump to rinse the total batch of hot water
    c. Do not let the pump run dry!
40. Refill the water tank with the prepared second batch of warm water, approx. 20 litre and add a little amount of detergent
41. Second rinse:
    a. Set to closed circuit using the 3-way valve
    b. Rinse the system for 5 minutes
    c. Set 3-way valve to open circuit
    d. Dispose the water. Do not let the pump run dry!
42. Clean the rinsing water tank
    a. Disconnect at the bottom to collect remaining water in bucket.
       Dispose appropriately.
    b. Open from the top and use additional water and paper to clean the inside
    c. Connect all parts again
    d. When the boiler is ready, prepare a third batch of hot water, approx. 25 litre
       No detergent

43. Clean the flow loop:
    a. Disconnect all pipes of the flow loop
    b. Use the cable and sponge attached to a rope to clean the 3 m measurement pipe
        i. Also use some additional water and detergent
        ii. Be careful to not make scratches on the inside of the pipe
    c. If necessary, repeat action b
    d. If necessary perform the action 43.b for the other parts (at least once a week)
    e. Clean the pipe connection from detergent residue
44. Re-attach the flow loop to the rinsing system
45. Third rinse
    a. Rinse in open circuit to flush away remaining detergent
    b. Stop halfway of the batch
    c. Use a syringe to flush both pressure tap connections
    d. Flush the remaining batch of water

5. Closure

46. Clean the table from liquids and paper
47. Disconnect the flow loop and dry the table (again)
    a. From experience, the pipes remained cleaner when disconnecting and let them dry. The bends can be placed vertically against the back wall for the oil to creep out
48. Plug out the pumps and boiler
49. Remove the nozzle from oil pumping and close the hole
50. Turn of the heating device, if applicable
51. Close the experiment water tap at the back
    a. Open and close the water tap on the divider, to dispose of the pressure in the water flow rate sensor
52. Close the main water supply valve
53. Turn off the power for the pressure transducer
54. Safe the data appropriately for post processing and turn of the computer when work is done
55. One has to wait for approx. 22 hours for the oil and water to separate and to perform a new experiment

6. Flow visualisation

The actual camera and computer can change between users. The following points will help for obtaining high quality images:

- Take time to align the camera with the imaging section.
  Keep checking the result on the screen.
- Also test when water is in the pipe. This can influence the image.
- Before an experiment:
  - Double check the settings for the frame rate, resolution and exposure time
  - After the zero pressure measurement, check the image with all light sources on.
- During an experiment:
  - The final duration of the recording is based on the frame rate. Know what and when you want to trigger.
  - When using the construction light as a source, only power it on just prior to the recording. It generates a lot of heat. And turn it off when the recording is finished.
  - The generated heat by the lamp, heats up the water in the visualisation and correction box. This can cause small air bubbles on the pipe wall and distort the image

About the visualisation box, mirror and correction box:

- Make sure no air bubbles are present in the visualisation box.
  At least not in the field of interest
- The mirror is a high quality first surface mirror. Use the cover to protect it
- The mirror is attached to the visualisation box using two-sided tape
- Align the correction box parallel to the visualisation box and remove air bubbles from the wall